Published April 16, 2018, doi:10.4049/jimmunol.1701605

Oral $NaHCO_3$ Activates a Splenic Anti-Inflammatory Pathway: Evidence That Cholinergic Signals Are Transmitted via Mesothelial Cells

Sarah C. Ray,* Babak Baban,† Matthew A. Tucker,‡ Alec J. Seaton,* Kyu Chul Chang,* Elinor C. Mannon,* Jingping Sun,* Bansari Patel,* Katie Wilson,* Jacqueline B. Musall,* Hiram Ocasio,* Debra Irsik,* Jessica A. Filosa,* Jennifer C. Sullivan,* Brendan Marshall,§ Ryan A. Harris,‡ and Paul M. O'Connor*

We tested the hypothesis that oral $NaHCO_3$ intake stimulates splenic anti-inflammatory pathways. Following oral $NaHCO_3$ loading, macrophage polarization was shifted from predominantly M1 (inflammatory) to M2 (regulatory) phenotypes, and $FOXP3^+CD4^+$ T-lymphocytes increased in the spleen, blood, and kidneys of rats. Similar anti-inflammatory changes in macrophage polarization were observed in the blood of human subjects following $NaHCO_3$ ingestion. Surprisingly, we found that gentle manipulation to visualize the spleen at midline during surgical laparotomy (sham splenectomy) was sufficient to abolish the response in rats and resulted in hypertrophy/hyperplasia of the capsular mesothelial cells. Thin collagenous connections lined by mesothelial cells were found to connect to the capsular mesothelium. Mesothelial cells in these connections stained positive for the pan-neuronal marker PGP9.5 and acetylcholine esterase and contained many ultrastructural elements, which visually resembled neuronal structures. Both disruption of the fragile mesothelial connections or transection of the vagal nerves resulted in the loss of capsular mesothelial acetylcholine esterase staining and reduced splenic mass. Our data indicate that oral $NaHCO_3$ activates a splenic anti-inflammatory pathway and provides evidence that the signals that mediate this response are transmitted to the spleen via a novel neuronal-like function of mesothelial cells. ***The Journal of Immunology*****, 2018, 200: 000–000.**

Chronic inflammation has been implicated in both acute and chronic kidney injury (1). The Chronic Renal Insufficiency Cohort study found that elevated inflammatory markers fibrinogen and TNF-α were associated with rapid loss of kidney function in patients with chronic kidney disease (CKD) (2). Furthermore, treatment with TNF-α antagonists has been associated with an attenuation in renal functional decline in CKD patients (3). Activation of the innate cholinergic anti-inflammatory pathway via stimulation of the vagal nerve, which suppresses proinflammatory cytokines and promotes anti-inflammatory macrophage cell polarization via activation of α-7-containing nicotinic receptors on splenic macrophages (4), has also been reported to ameliorate acute kidney injury (5).

Evidence from a number of small clinical trials as well as experimental models indicates that supplementation with oral sodium bicarbonate ($NaHCO_3$) may slow the decline in kidney function in CKD patients (6), yet the physiological mechanisms mediating this beneficial effect remain unclear. As inflammation has been associated with CKD progression, we speculated that $NaHCO_3$ may act to protect the kidneys by reducing inflammation. Therefore, we tested the hypothesis that "Oral $NaHCO_3$ intake promotes M2 macrophage polarization by activating splenic anti-inflammatory pathways."

In the current study, we used flow cytometry as well as mRNA markers in isolated splenic macrophages to determine whether oral $NaHCO_3$ intake promotes M2 macrophage polarization in the kidney and spleen in both hypertensive Dahl salt-sensitive (SS) rats, in which significant inflammation is known to be present (7), as well as normotensive Sprague Dawley rats, in which baseline renal inflammation has been reported to be low. We also investigated the effect of acute oral $NaHCO_3$ loading on inflammatory cell profiles in the blood of healthy human subjects. Furthermore, as we found that gentle manipulation to visualize the spleen at midline during surgical laparotomy (sham splenectomy) was sufficient to abolish the anti-inflammatory response to oral $NaHCO_3$, we investigated the pathways through which signaling of $NaHCO_3$ intake may be transmitted to the splenic parenchyma.

Materials and Methods

Rodent studies

Animals. Studies used 8–12-wk-old male Dahl SS or Sprague Dawley rats (Charles River Laboratories, Wilmington, MA). Rats were maintained ad libitum on water and a pellet diet containing low 0.4% NaCl (AIN76A; Dyets, Bethlehem, PA; low salt [LS] 0.4% NaCl). Rats were age matched for all protocols. All studies were conducted in accordance with the National Institutes of Health Guide for the Care and Use of Laboratory

*Department of Physiology, Augusta University, Augusta, GA 30912; †Department of Oral Biology, Augusta University, Augusta, GA 30912; ‡Georgia Prevention Institute, Augusta University, Augusta, GA 30912; and §Department of Cell Biology and Anatomy, Augusta University, Augusta, GA 30912

ORCIDs: 0000-0002-4698-3482 (A.J.S.); 0000-0002-8379-7144 (E.C.M.); 0000-0001-7536-2039 (J.A.F.); 0000-0001-7147-0075 (B.M.); 0000-0002-8826-681X (R.A.H.); 0000-0002-5632-8385 (P.M.O.).

Received for publication November 21, 2017. Accepted for publication March 10, 2018.

This work was supported by National Institutes of Health Grants DK099548 and 1P01HL134604 (to P.M.O.).

Address correspondence and reprint requests to Dr. Paul M. O'Connor, Augusta University, CB2206, 1459 Laney-Walker Boulevard, Augusta, GA 30912. E-mail address: paoconnor@augusta.edu

The online version of this article contains supplemental material.

Abbreviations used in this article: BMI, body mass index; CKD, chronic kidney disease; CON, control; GFR, glomerular filtration rate; HS, high salt; LS, low salt; MLA, methyllycaconitine; RT, room temperature; SS, salt-sensitive; Treg, T regulatory cell; TXT, treatment.

Animals. All of the protocols were approved in advance by the institutional animal care committee at Augusta University.

Sub diaphragmatic transection of the vagal nerves. Rats were anesthetized with isoflurane (2–5%), and a midline incision was performed. Using a stereoscope, the vagal nerves were visualized immediately below the diaphragm and transected. Any nervous tissue around the esophagus was also cleared by dissection. When visualizing the esophagus, care was taken to limit any horizontal movement of the stomach and to avoid movement of the spleen. After wound closure, animals were allowed to recover for 2 wk before tissue was harvested under isoflurane anesthesia. Bloating of the stomach was used to confirm sub diaphragmatic transection of the vagal nerves at the time of sacrifice.

Visualization of the spleen at midline or sham splenectomy. Dahl SS rats were anesthetized with isoflurane (2–5%), and a midline incision was performed. The spleen was located and gently moved toward the incision site by hand or with cotton tip applicators. The poles of the spleen were visualized and the spleen returned to its original position. Following the surgical procedure, rats were allowed to recover for 7 d before entering the high-salt (HS) protocol described above.

Drugs. Esomeprazole (20 mg/kg; Sigma, St Louis, MO) was dissolved in DMSO before being diluted in saline and given as a final volume of 0.2 ml i.p. once daily. Methyllycaconitine (MLA: 5 mg/kg; Sigma) was dissolved in saline and given i.p. (0.2 ml twice a day). Control rats received DMSO and saline as vehicle (0.2 ml i.p. twice a day). All rats in drug treatment protocols received either 0.1 M $NaHCO_3$ or NaCl in drinking water and were treated daily for 3 d prior to tissue harvest.

Analytical flow cytometry (rats). With the exception of one group of rats ($n = 5 + 5$), in all HS-fed Dahl SS rats, blood pressure telemetry devices were implanted prior to beginning the study. All protocols were initiated at least 7 d after surgery to allow time for rats to recover, and no significant differences in flow cytometry results were observed between rats that had telemeters implanted compared with rats without prior surgery. No surgical procedures were performed on LS-fed Dahl SS rats or Sprague Dawley rats prior to tissue harvest. On the day of tissue harvest, rats were anesthetized with isoflurane (2–5%), and a midline incision was performed. The abdominal aorta was catheterized for the collection of ~2 ml of arterial blood in a heparinized tube, and the left kidney was excised and immediately processed for flow cytometry. Ab markers used for flow cytometry as well as dilutions and references are given in Table I.

To identify and evaluate immune cells in renal and splenic tissues, we employed a flow cytometry-based assay. Briefly, kidneys were harvested and placed in RPMI 1640 (Thermo Fisher Laboratories) + 10% FBS (Atlanta Biologicals, Lawrenceville, GA), minced, and single-cell suspensions were achieved using a 100 μM cell strainer (BD Biosciences, San Diego, CA) followed by centrifugation (1400 rpm, 5 min) and lysis of erythrocytes by incubation with ACK Lysing Buffer (3 min at room temp; Quality Biological, Gathersburg, MD). Spleens were harvested and placed in RPMI 1640 + 10% FBS. Spleens were then injected with 1 ml of 100 collagen digestion units/ml Collagenase IV (Sigma) solution in three regions, then placed in 1 ml of 400 collagen digestion units/ml Collagenase IV, incubated at 37˚C for 30 min, and minced. Single-cell suspensions were then achieved as described for the kidney, and all cells were washed twice (PBS).

In all flow studies, cells were then incubated with Abs for surface markers for 20 min on ice in the dark (all Abs from Pharmingen-BD-Biosciences, San Jose, CA). Cells were then washed with PBS, fixed and permeabilized using FOXP3/Transcription Factor Fix/Perm Buffer (eBioscience, San Diego, CA) for 15 min in the dark on ice, and washed once again with PBS before incubation with Abs for intracellular staining of Foxp3, TNF-α, IL-10, and IL-17, on ice in the dark for 20 min (BD Biosciences). Cells were then washed and run through a four-color flow cytometer (FACS Calibur; Becton-Dickinson), and data were collected using CellQuest software.

In all flow studies, group identifiers were removed and flow cytometry analysis was performed by an investigator unaware of the hypothesis. Samples were double stained with control IgG and cell markers and were used to assess any spillover signal of fluorochromes; proper compensation was set to ensure the median fluorescence intensities of negative and positive cells were identical and were both gated populations. Gating was used to exclude dead cells and debris using forward and side scatterplots. In each analysis, 100,000 total events were collected. As a gating strategy, for each sample, isotype-matched controls were analyzed to set the appropriate gates. For each marker, samples were analyzed in duplicate measurements. To minimize false-positive events, the number of double-positive events detected with the isotype controls was subtracted from the number of double-positive cells stained with corresponding Abs (not isotype control), respectively. Cells expressing a specific marker were reported as a percentage of the number of gated events. A representative example of gating is shown in Fig. 1 and Supplemental Fig. 2.

Verification of macrophage polarization in isolated splenic macrophages. Markers for M1 and M2 macrophages were selected based on previous studies in the rat (8, 9); however, to confirm the specificity of these markers, in a subset of animals, these markers were compared with alternative markers (Supplemental Fig. 2) and depletion of kidney cells identified as macrophages was confirmed using clodronate liposomes (Supplemental Fig. 3). In these studies, a single dose of clodronate liposomes or liposome controls (20 mg/kg; Encapsula Nanosciences, Nashville, TN) was injected into the tail vein of rats 24 and 72 h prior to harvesting the kidneys for flow cytometry. In addition, rat spleen macrophages were isolated from Dahl SS rats treated with either NaCl or $NaHCO_3$ for 2 wk and fed an HS (8%) diet. Splenic macrophages were isolated by centrifugation in a Percoll density gradient and real-time PCR was performed for rat iNOS, arginase, and GAPDH to determine relative M1/M2 macrophage polarization.

MLR. The MLR is a commonly used functional assay to determine the proliferative capacity of T lymphocytes in response to Ag presentation. This assay requires the use of responder cells (T cells from the spleen of untreated Dahl SS rats) and stimulating cells (splenocytes) from Sprague Dawley rats drinking either NaCl (0.1 M) or $NaHCO_3$ (0.1 M) for 3 d prior to tissue harvest ($n = 3$ animals each group). The responder cells and stimulator cells were set up in triplicate wells in a RPMI 1640 medium, which was supplemented with FBS, penicillin, streptomycin, *l*-glutamine, and 2-ME. Responder T cells were enriched using magnetic assorted cell sorting and used at the ratio of 1:5 (responders to stimulators). After 96 h of incubation at 37˚C in a humidified 5% CO_2 environment, all cells were harvested into flow cytometry tubes. After one wash with PBS, all samples were then incubated with anti- CD71 Ab (a marker for activated and dividing T cells) for 20 min in the dark on ice. Samples were then washed with PBS, and T-cell proliferation was measured by using flow cytometry analysis for CD71 expression. The average of the triplicate samples was recorded for each rat, and the average of all animals in each group then calculated and compared by unpaired *t* test.

Isolation of primary macrophage from spleen and polarization by arginase/iNOS. Real-time PCR was performed using rat iNOS, arginase, and GAPDH primers listed below, as previously reported (9): 1) rat iNOS forward 5′-TCT TGG TGA AAG CGG TGT T-3′; 2) rat iNOS reverse 5′-TGT TGC GTT GGA AGT GTA GC-3′; 3) arginase forward 5′-TAT CTG CCA AGG ACA TCG TG-3′; and 4) arginase reverse 5′-GTT CTG TTC GGT TTG CTG T-3′.

For urine collection, rats were placed in rat metabolic cages for 24 h (Nalgene, Rochester, NY). Urine was collected and weighed for volume determination. Up to 10 ml of urine was stored at −80˚C for later analysis. All urinary data are presented as 24 h urinary excretion. Urinary Na, K, and Cl measurements were obtained using an electrolyte analyzer (Easylite; Medica, Bedford, MA). Samples were diluted 1:10, one part urine to nine parts Easylyte Urine Diluent as per the manufactures instructions. Urinary titratable acids were determined with titration of 5 ml of urine with NaOH or HCl to pH 7.4. Urinary NH_4^+ concentration was determined using an ammonia ion selective electrode (Orion high performance ammonia ion selective electrode [Thermo Fisher Scientific]). Urine samples were diluted in Orion ionplus Solution Alkaline Reagent immediately before measurement as per the manufacturer's instructions. Measurements were compared with those of a standard curve using serial dilutions of the Thermo Scientific Orion Application Solution 0.1 M NH_4^+ Ammonium Standard. Final concentrations were calculated using a log curve (Graphpad Prism 6; Graphpad Software, La Jolla, CA).

Electron microscopy. Preparation and imaging of tissue by electron microscopy was performed by the Augusta University Histology Core facility. Tissue was fixed in 4% paraformaldehyde, 2% glutaraldehyde in 0.1 M sodium cacodylate (NaCac) buffer, pH 7.4, postfixed in 2% osmium tetroxide in NaCac, stained en bloc with 2% uranyl acetate, dehydrated with a graded ethanol series, and embedded in Epon-Araldite resin. Thin sections of 75 nm thickness were cut with a diamond knife on a Leica EM UC6 ultramicrotome (Leica Microsystems, Bannockburn, IL), collected on copper grids, and stained with uranyl acetate and lead citrate. Tissue was observed in a JEM 1230 transmission electron microscope (JEOL USA, Peabody, MA) at 110 kV and imaged with an UltraScan 4000 CCD camera and First Light Digital Camera Controller (Gatan, Pleasantonm, CA).

Histological analysis. At the end of the study, rats were anesthetized with isoflurane (2–5%), and tissues were excised and placed in 10% formalin solution (Sigma) for 48 h before being paraffin embedded, blocked, and processed (Augusta University Core facility). Kidneys were paraffin embedded in an automatic tissue processor, and 3-μm cut sections were mounted on siliconized and/or charged slides. The slides were deparaffinized and hydrated, and Ag retrieval was performed using IHC-Tek Epitope retrieval solution at steaming for 40 min (catalog no. IW-1100;

IHCWorld). Tissue was blocked with 3% hydrogen peroxide in methanol for 10 min. The primary Abs used are listed in the Table I. The goat anti-rabbit IgG-HRP–conjugated secondary Ab (catalog no. sc-2004, 400 μg/ml, 1:400 at 1 μg/ml; Santa-cruz) was used for 30 min at room temperature (RT). The slides were stained with Betazoid DAB Chromogen Kit (catalog no. BDB2004H; Biocare Medical). Omitting the first Ab served as a negative control and resulted in no positive staining in tissue. All end-point analysis was blinded to the investigators. For histological scoring, all identifiers were removed, and slides were given a number before being scored by an investigator that was unaware of the hypothesis being tested. Data were then compiled by the primary investigator who had access to the numbering key.

Ca^{2+} imaging. Untreated rats were anesthetized with isoflurane (2–5%), and the spleen was excised. The spleen was placed in HBSS with 20 mM HEPES buffer pH 7.40 at RT with Fluo4. Imaging acquisition was conducted using the Andor Revolution system (Andor Technology Belfast, U.K.) (10). A Nikon microscope (Eclipse FN 1; Nikon, Tokyo, Japan) was connected to a laser confocal spinning unit (CSU-X1; Yokogawa, Tokyo, Japan) attached to a Sutter filter wheel and an ultrasensitive EMCCD camera (iXon^{EM}; Andor Technology, Belfast, U.K.). The microscope chamber was continuously perfused, at a rate of 2 ∼3 ml/min, with HBSS pH 7.4 using a peristaltic pump (Miniplus 3; Gilson, Middleton, WI). Chamber temperature was maintained at 36 ± 1°C using a single line solution heater (SH-28B; Warner Instruments, Hamden, CT) connected to a direct current power supply (1735A; BK Precision, Yorba Linda, CA). Calcium imaging experiments were monitored from thick spleen slices incubated at RT in HBSS containing 5 μM Fluo-4 AM and pluronic acid (2.5 μg/ml). Following an hour incubation period, slices were placed in RT HBSS until needed. Fluorescence images were obtained using a krypton/argon laser (488 nm excitation and >495 nm emission). Images were acquired at ∼0.7 frames/s. 40× or 20× Nikon dipping objectives were used to visualize the spleen surface during electrical stimulation.

Rat protocols. All rats were maintained on LS chow with ad libitum water (tap water). Following 7 d recovery from surgery, on day 1 of the HS diet protocol, tap water was replaced with either 0.1 M $NaHCO_3$ ($n = 11$; Sigma) or equimolar NaCl (0.1 M) made fresh daily, also ad libitum ($n = 10$). $NaHCO_3$ or vehicle-treated water was then maintained for the remainder of the protocol. Following 4 d of LS feeding, rats were placed on an 8% HS diet (AIN76A 8%; Dyets) for 2 wk. Twenty-four-hour urine collections were obtained on day 3 of LS feeding and day 7 and day 14 of HS feeding, if applicable. Following 14 d of HS feeding, rats were anesthetized with isoflurane (2–5%), and tissue was harvested for analysis.

Dahl SS rats on the LS protocol were treated identically to the HS protocol above except following 4 d of LS, rats were anesthetized and tissue was harvested for flow cytometric analysis prior to beginning an HS diet. $n = 5/5$ for NaCl and $NaHCO_3$ treatment, respectively.

Subdiaphragmatic transection of the vagal nerves was as follows: 8-wk-old Sprague Dawley rats were either subject to laparotomy only, laparotomy + manipulation of the spleen to midline, or laparotomy + transection of the vagal nerves immediately below the diaphragm or laparotomy + transection of the vagal nerves immediately below the diaphragm + manipulation of the spleen to midline. Rats were allowed to recover for 14 d before being anesthetized with isoflurane (2–5%) and tissue harvested. Successful transection of the vagal nerves was confirmed by stomach bloating on sacrifice, and animals without confirmation were excluded from analysis.

Visualization of the spleen at midline or sham splenectomy. Dahl SS rats in which the spleen was removed ($n = 5/7$ for vehicle and $NaHCO_3$ treatment, respectively) or moved to midline during surgery (sham splenectomy [$n = 5/5$ for vehicle and $NaHCO_3$ treatment, respectively]) were entered into the HS protocol described above prior to tissue sacrifice. An additional sham control (CON) group (laparotomy only) was performed to control for movement of the spleen ($n = 4/5$ for vehicle and $NaHCO_3$ treatment, respectively). Tissue collected from animals in this group was used to compare Ab sets for identification of macrophage polarization (Supplemental Fig. 2).

Dose response studies in Sprague Dawley rats. Rats were maintained on standard laboratory chow (Teklad) and placed on either 0.1 M $NaHCO_3$, 0.05 M NaCl/0.05 M $NaHCO_3$, 0.09 M NaCl/0.01 $NaHCO_3$, or 0.1 M NaCl for 4 d prior to tissue harvest ($n = 3$ animals were used at each dose).

Human studies

Participants. To examine the effects of $NaHCO_3$ on acute changes in parasympathetic activity, 12 healthy participants (six men, six women, age 27 ± 2 y, body mass index [BMI] 25.3 ± 1.2 kg/m^2) were provided 2 g of $NaHCO_3$ dissolved in 250 ml of bottled water (treatment [TXT] group). An additional six participants (four men, two women, age 25 ± 1, BMI 25.7 ± 2.1 kg/m^2) were recruited as controls and were provided 1.39 g of NaCl (equivalent molar load to 2 g of $NaHCO_3$) dissolved in 250 ml of bottled water (CON group).

Serum electrolytes. Blood samples were collected via an i.v. catheter (Nexiva; Becton Dickinson, Franklin Lakes, NJ) at baseline and at 60 min intervals posttreatment to examine changes in serum electrolyte balance (Na, K, and Cl^-).

Analytical flow cytometry (humans). In the $NaHCO_3$ TXT group, 10 of 12 subjects had blood drawn at 3 h posttreatment. Blood was taken at all time points for all control subjects. No data were excluded from the analysis. Flow cytometric analysis of heparinized whole blood was performed as described previously (11–13). Briefly, cells were incubated with Abs for surface markers (15 min on ice in dark) before incubation with Abs against intracellular cytokines and factors (after permeabilization for 15 min using fix/Perm mixture; eBioscience), including CD11b, CD68, TNF-α (for M1 macrophages); CD11b, CD68, CD206 and IL-10 (for M2 macrophages) (purchased from BD BioSciences); and CD16 and TNF-α (for neutrophils; from eBioscience). Cells were then washed and run through a four-color flow cytometer (FACS Calibur; BD Biosciences), and data were collected using CellQuest software. Samples were double-stained with control IgG and cell markers to assess any spillover signal of fluorochromes. Proper compensation was set to ensure the median fluorescence intensities of negative and positive cells were identical and then was used to gate the population. Gating excluded dead cells and debris using forward and side scatter plots. To confirm the specificity of primary Ab binding and rule out nonspecific Fc receptor binding to cells or other cellular protein interactions, negative control experiments were conducted using isotype controls matched to each primary Ab's host species, isotype, and conjugation format. The control Abs had no specificity for target cells within our studies yet retain all the nonspecific characteristics of the Abs used in the experiments.

Statistics and analysis

Data were analyzed using Graphpad Prism (Graphpad) software. All data are expressed as mean ± SE. Multiple comparisons were analyzed using two-way ANOVA. All other parametric comparisons were analyzed via unpaired two-sided Student t test. Categorical data were analyzed by Fisher exact test. Significance was considered to be $p < 0.05$. All end point analysis was blinded to the investigators at the time of measurement and compiled using an identifier key once analysis was complete. No data were excluded following end point analysis (some animals were excluded prior to analysis that met exclusion criteria, i.e., failure to confirm vagal denervation). Flow cytometry gating and analysis was performed by an investigator who was unaware of the hypothesis being tested. Rats were received from a commercial source (two to three rats per cage) and were randomly allocated to either vehicle or treatment, taking care to allocate at least one animal per cage to each group.

The study followed the principles of the Declaration of Helsinki. All study protocols were approved by the Human Assurance Committee at Augusta University (no. 1029130), and written and verbal informed consent was received from all participants prior to inclusion in the study.

Results

Rat studies

Electrolytes. Urine electrolytes were measured in HS-fed (8% NaCl chow) Dahl SS rats. The addition of $NaHCO_3$ (0.1 M) to the drinking water of Dahl SS rats had no effect on urinary Na or K excretion when compared with vehicle (0.1 M NaCl), indicating similar Na and K intake across the course of the study. Urinary Cl excretion was significantly lower ($p = 0.03$) in rats drinking $NaHCO_3$ solution, reflecting that a large portion of Na intake in these animals was from $NaHCO_3$.

Inflammatory profile. Immune cell profiles were identified using Ab markers listed in Table I. Flow cytometry data from blood, spleen, and whole kidney of rats treated with either vehicle or $NaHCO_3$ after 2 wk of HS are presented in Table II. $NaHCO_3$ treatment resulted in a significant ($p < 0.01$) decrease in TNF-α–expressing macrophages (M1-polarized macrophages) and an increase in IL-10–expressing macrophages (M2-polarized macrophages) in the kidney (Fig. 1, Table II; $p < 0.04$). A significant ($p = 0.005$) polarization from predominately M1 to M2

Table I. Abs and reagents

Ab Name	Company	Catalog No.	Lot No.	Tube Amount	Information	Ab Validation
CD3- PerCP	eBioscience	46-0030-82	E16590-104	0.5 ml, 100 μg	Anti-rat	(59)
CD4-FITC, OX-35	BD Biosciences	554837	5190753	0.5 ml, 100 μg	Mouse anti-rat	(33)
FOX P3-APC	eBioscience	17-5773-82	E07303-1639	0.5 ml, 100 μg	Anti-mouse/rat	(59)
RORγ/RORC- PE	R&D Systems	IC6006P	ABHO0214091		Mouse IgG	(33)
CD11b/c-PE, OX-42	BD Pharmingen	554862		1.0 ml	Anti-rat	(60)
CD11b/c-PE, OX-42	eBioscience	12-0110-80	E15919-106	125 μl/500 μl	Anti-rat	(61)
CD206 PerCP/Cy 5.5	BioLegend	321122	B175845	0.5 ml	Anti-human	(62)
F4/80-A488, EMRI	Bioss	bs-7058R-A488	AE084243	100 μl	Rabbit	http://biossusa.com/store/datasheets/bs-7058R-A488
IL-10-Alexa647, CC320	Novus	NB100-63026AF6477	1007-081415	250 μl	Mouse ab	http://www.novusbio.com/IL-10-Antibody-CC320_NB100-63026AF647.html
CD44-FITC, OX-49	BD Biosciences	550974	4324539	0.2 ml	Mouse anti-rat	(32, 33)
CD69-PE, H1.2F3	eBioscience	12-0691-82	E01332-1634	0.5 ml	Anti-mouse	(63)
TNF-α-biotin	Bioss	bs-2081R-biotin	AE081731	100 μl	Rabbit	http://biossusa.com/store/bs-2081r-biotin.html
IL-17A-PE	eBioscience	12-7177-81	4276914	0.25 ml	Anti-mouse/rat	(64)
CD68-FITC	Bio-Rad	MCA341F	1601	1.0 ml	Mouse anti-rat monoclonal	(65)
CD163-Alexa 647	AbD Serotec	MCA342A647	913	1.0 ml	Mouse anti-rat monoclonal	(66)
IL-10-PE	BD Pharmingen	555088	8021822	500 μl	Mouse anti-rat monoclonal	http://bdbiosciences.com/pe, mouse anti-rat IL10-555088
Streptavidin-APC	eBioscience	17-4317-82	E07261-1634	0.5 ml		http://www.ebioscience.com/media/pdf/tds/17/17-4317.pdf
FIX/Perm Buffer/FOXP3 fixation	eBioscience	NC9548464/00-5521-00	E00027-1654			(67)
Collagenase IV	Sigma	C5138-500 mg		500 mg		(67)
ACK Lysing Buffer	Quality Biological	50983220		4 × 100 ml		(67)
CD11b-FITC	BD Biosciences	78022	B202614			
CD68-FITC	BD Biosciences	562117	2219733			(68)
TNF-α−PE	eBioscience	12-7349-82	E02153-1634			(69)
CD206-APC	BioLegend	321109	B202690			(70)
IL-10-APC	BioLegend	506806	B244158			(71)
Tyrosine hydroxylase	Abcam	Ab112	GR286793-6	100 μl (0.5 mg/ml)		(72)
Acetylcholine esterase	Invitrogen	PA5-21371	SC2362081N	100 μl (1 mg/ml)		
PGP9.5	Sigma	SAB4503057	310302	100 μg		

All Abs used in flow cytometry and immunohistochemical studies along with reagents are listed in the table.

Table II. Rat flow cytometry

	CD3 (% total kidney)	CD4 (% CD3)	CD44 (% CD3)	CD69 (% CD3)	FOXP3 (% CD3/CD4)	IL-17 (% total kidney)	M1 (% total kidney)	M2 (% total kidney)	IL-10 (% total kidney)	TNF-α (% total kidney)	CD11b/c (% total kidney)
14 d HS											
Blood											
Vehicle (n = 4)	54 ± 1	55 ± 2	19 ± 2	1.2 ± 0.3	2.5 ± 0.3	8 ± 1					
Bicarbonate (n = 5)	57 ± 2	53 ± 2	14 ± 2	0.9 ± 0.3	4.4 ± 0.6	6 ± 1					
p	NS	NS	NS	NS	0.02[a]	NS					
Kidney											
Vehicle (n = 10)	2.1 ± 0.3	57 ± 1	47 ± 4	1.8 ± 0.4	1.7 ± 0.3	1.1 ± 0.2	0.26 ± 0.03	0.12 ± 0.02	2.8 ± 0.3	3.2 ± 0.4	0.29 ± 0.04
Bicarbonate (n = 11)	1.8 ± 0.3	55 ± 2	36 ± 5	2.8 ± 0.7	3.3 ± 0.5	0.7 ± 0.1	0.12 ± 0.02	0.20 ± 0.03	4.2 ± 0.3	2.0 ± 0.3	0.40 ± 0.04
p	NS	NS	NS	NS	0.01[a]	NS	0.001**	0.04[a]	0.048[a]	0.03[a]	NS
3 d LS											
Blood											
Vehicle (n = 5)	57 ± 1	54 ± 1	15 ± 2	2.4 ± 0.7	4.8 ± 0.8	5.4 ± 0.5					
Bicarbonate (n = 5)	57 ± 2	55 ± 1	18 ± 1	1.6 ± 0.5	5.8 ± 0.7	5.6 ± 1.1					
p	NS	NS	NS	NS	NS	NS					
Kidney											
Vehicle (n = 5)	1.1 ± 0.2	59 ± 1	58 ± 1	0.9 ± 0.1	1.6 ± 0.2	1.3 ± 0.5	0.30 ± 0.06	0.20 ± 0.05	3.0 ± 0.5	2.4 ± 0.5	0.22 ± 0.06
Bicarbonate (n = 5)	1.1 ± 0.3	54 ± 2	52 ± 3	0.9 ± 0.3	2.6 ± 0.5	0.4 ± 0.2	0.16 ± 0.04	0.36 ± 0.02	4.8 ± 0.5	1.4 ± 0.2	0.24 ± 0.02
p	NS	0.02[a]	NS (0.07)	NS	NS	NS	NS (0.1)	0.03[a]	0.04[a]	NS (0.11)	NS
14 d HS											
Spleen											
Vehicle (n = 5)	15.8 ± 0.8	57 ± 1	40 ± 2	5.2 ± 0.7	4.2 ± 0.2	4.4 ± 0.5	8.6 ± 0.7	6.4 ± 0.5	5.8 ± 0.8	5.8 ± 0.8	6 ± 0.4
Bicarbonate (n = 6)	15.3 ± 0.8	53 ± 1	35 ± 2	7.2 ± 0.9	6 ± 0.5	2.8 ± 0.6	5.8 ± 0.5	8.3 ± 0.5	7.5 ± 0.7	3 ± 0.5	7.3 ± 0.6
p	NS	NS (0.06)	0.04[a]	NS	0.015[a]	NS (0.08)	0.01[a]	0.02[a]	NS	0.01[a]	NS

All data from flow cytometric analyses of blood and kidneys from Dahl SS rats drinking either 0.1 M $NaHCO_3$ (bicarbonate) or equimolar NaCl (vehicle) are presented in the table. Data from 14 d HS and 3 d only LS-fed animals are shown. All groups represent n = 4–11, with absolute numbers for each group presented in the table. p is the result of unpaired Student t test comparing vehicle- and bicarbonate-treated groups. Two studies were pooled for HS kidney analysis. In group 1 (n = 5 + 5), blood and kidney samples were analyzed from Dahl SS rats fed an HS diet for 14 d that did not have prior surgery. In group 2 (n = 5 + 6 for vehicle and bicarbonate, respectively), kidney and spleen were analyzed. Blood pressure (telemetry), urine analysis, and histological measurements of injury were all performed in group 2 animals. CD3-, IL-17–, Il-10–, M1-, M2-, TNF-α–, and CD11b/c-positive cells are all expressed as the percentage of total kidney or spleen cells ± SE. CD4-, CD44-, and CD69-positive cells are expressed as the percentage of CD4-positive cells. FOXP3-positive cells are expressed as the percentage of both CD3- and CD4-positive cells.

[a]For all analyses, $p < 0.05$ was considered significant.

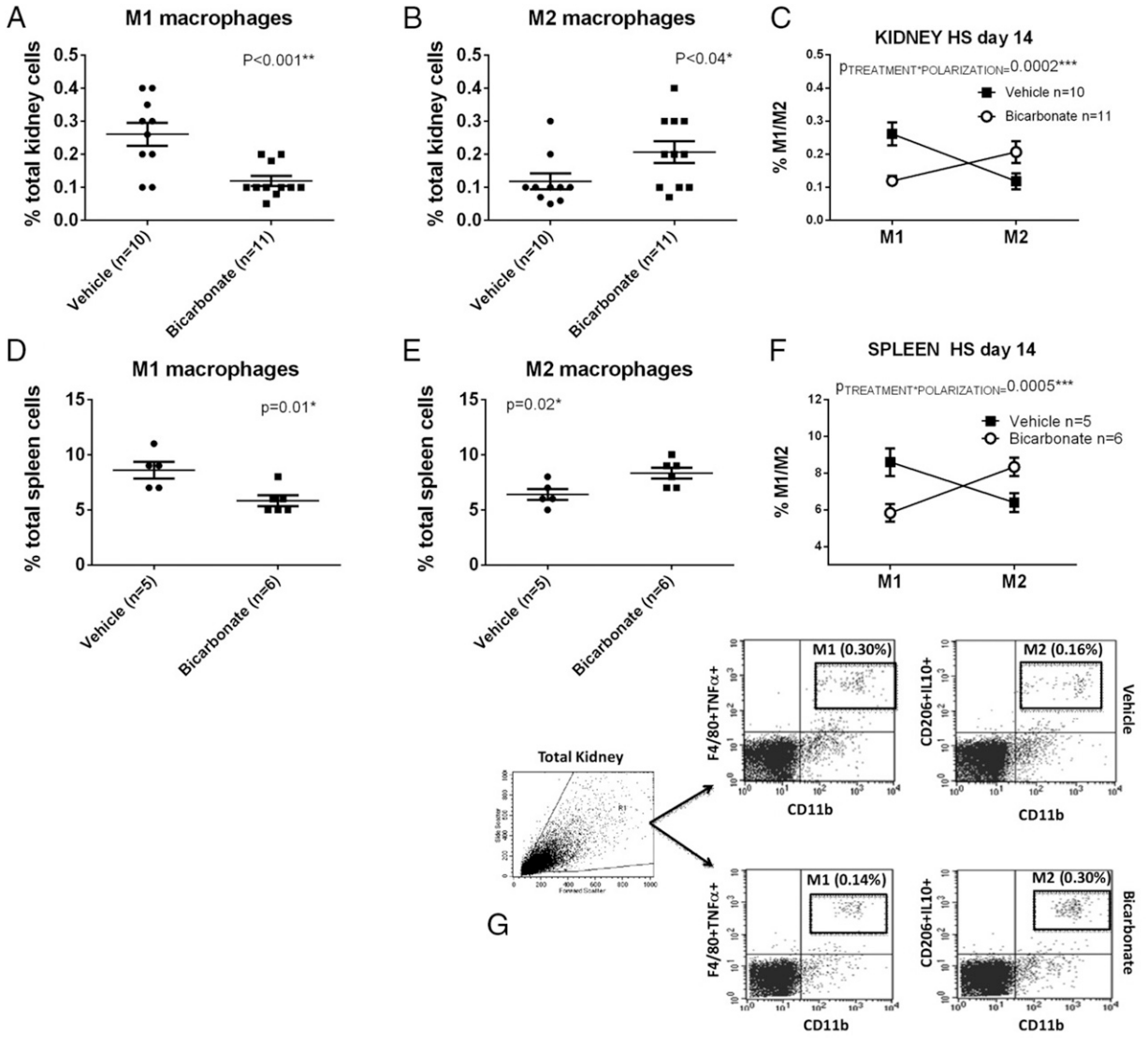

FIGURE 1. Data from flow cytometric analysis of macrophage polarization (M1/M2) from kidneys and spleen from male Dahl SS rats drinking 0.1 M $NaHCO_3$ (bicarbonate) or equimolar NaCl (vehicle) are presented in (**A**)–(**G**). All data are from rats placed on treated water (vehicle or bicarbonate) for 3 d before being switched to an HS diet for 14 d prior to tissue harvest. (A) The percentage of total kidney cells identified as M1 macrophages (CD11b/F4/80$^+$/TNF-α^+ cells) in vehicle- (n = 10; filled circles) and bicarbonate- (n = 11; filled squares) treated rats. (B) The percentage of total kidney cells identified as M2 macrophages (CD11b/CD206$^+$/IL10$^+$ cells) in vehicle- (n = 10; filled circles) and bicarbonate- (n = 11; filled squares) treated rats. (C) Relative expression of M1 and M2 macrophages expressed as a percentage of total kidney cells in vehicle- (filled squares) and bicarbonate- (open circles) treated rats. (D) The percentage of total spleen cells identified as M1 macrophages (CD11b/F4/80$^+$/TNF-α^+ cells) in vehicle- (n = 10; filled circles) and bicarbonate- (n = 11; filled squares) treated rats. (E) The percentage of total spleen cells identified as M2 macrophages (CD11b/CD206$^+$/IL10$^+$ cells) in vehicle- (n = 10; filled circles) and bicarbonate- (n = 11; filled squares) treated rats. (F) Relative expression of M1 and M2 macrophages expressed as percentage of total spleen cells in vehicle- (filled squares) and bicarbonate- (open circles) treated rats. (G) Representative gating images from kidneys of HS-treated rats.

macrophage polarization was also observed in splenic tissue of HS-fed Dahl SS rats treated with $NaHCO_3$ (Fig. 1, Table II). The percentage of T cells identified as FOX3$^+$CD4$^+$ T cells in the spleen, kidney, and blood of $NaHCO_3$-treated rats was also significantly increased when compared with NaCl-treated rats (Table II).

As the Dahl SS rat model develops hypertension and renal injury when fed an HS diet (14), to determine whether $NaHCO_3$ promotes anti-inflammatory responses independent of these changes, we examined tissues from LS-fed Dahl SS rats and normotensive Sprague Dawley rats. Importantly, in LS-fed Dahl SS rats, a significant (p = 0.007) polarization from predominately M1 to M2 macrophage polarization was still observed in kidney tissue (Fig. 2). Furthermore, we found that the effect of $NaHCO_3$ intake to promote M2 polarization in the kidney was also observed in outbred Sprague Dawley rats (Fig. 2). The effect of $NaHCO_3$ was found to be dose dependent, with changes in macrophage polarization identified with as little as 0.01 M $NaHCO_3$ in the drinking water following only 4 d of $NaHCO_3$ drinking in rats eating LS laboratory chow (Fig. 2).

Human subjects

To determine whether oral $NaHCO_3$ had a similar anti-inflammatory action in humans as we found in rats, we evaluated blood samples at baseline and 1, 2, and 3 h following ingestion of a single dose (2 g) of $NaHCO_3$ (n = 11) or equimolar NaCl (n = 6), each dissolved in 250 ml of bottled water. Pre- and posttreatment values of serum electrolytes are presented in Table III. There was a significant group by time interaction for

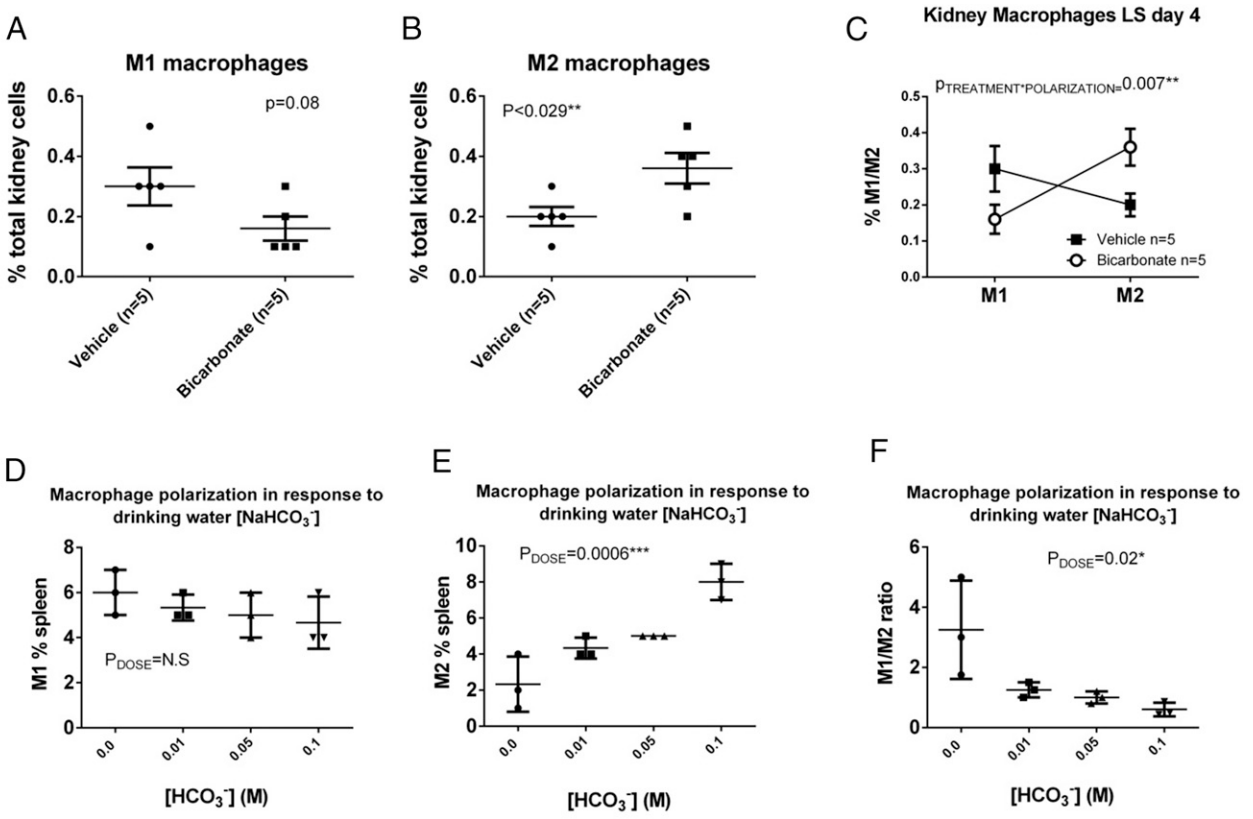

FIGURE 2. Data from flow cytometric analysis of macrophage polarization (M1/M2) from kidneys and spleens from male Dahl SS rats drinking either 0.1 M $NaHCO_3$ (bicarbonate) or equimolar NaCl (vehicle) are presented in (**A**)–(**C**). All data are from rats placed on treated water (vehicle or bicarbonate) for 3 d before tissue harvest. (A) The percentage of total kidney cells identified as M1 macrophages (CD11b/F4/80$^+$/TNF-α^+ cells) in vehicle- (n = 5; filled circles) and bicarbonate- (n = 5; filled squares) treated rats. (B) The percentage of total kidney cells identified as M2 macrophages (CD11b/CD206$^+$/IL10$^+$ cells) in vehicle- (n = 5; filled circles) and bicarbonate- (n = 5; filled squares) treated rats. (C) Relative expression of M1 and M2 macrophages expressed as the percentage of total kidney cells in vehicle- (filled squares) and bicarbonate- (open circles) treated rats. (**D**–**F**) Data from flow cytometric analysis of macrophage polarization (M1/M2) in kidneys of male Sprague Dawley rats (Charles River Laboratories) drinking either 0.1 M $NaHCO_3$ (n = 3), 0.05 M $NaHCO_3$/0.05 M NaCl (n = 3), 0.01 M $NaHCO_3$/0.09 M NaCl (n = 3), or 0.1 M NaCl (n = 3) for 4 d prior to tissue harvest. All rats were fed standard laboratory chow (Teklad). (D) The percentage of total kidney cells identified as M1 macrophages (CD11b/F4/80$^+$/TNF-α^+ cells) in response to increasing concentrations of$NaHCO_3$ in drinking water (0 M on right to 0.1 M on left). All doses were made equimolar with the addition of NaCl to the drinking water. (E) The percentage of total kidney cells identified as M2 macrophages (CD11b/CD206$^+$/IL10$^+$ cells) in response to increasing concentrations of $NaHCO_3$ in drinking water (0 M on right to 0.1 M on left). (F) Ratio of M1 to M2 macrophages expressed as the percentage of total kidney cells in response to increasing concentrations of $NaHCO_3$ in drinking water.

changes in serum potassium (p = 0.029, η_p^2 = 0.279). Specifically, serum potassium decreased with $NaHCO_3$ treatment (p = 0.008), but there was no change with NaCl treatment (p = 0.381). BMI and C-reactive protein levels were not significantly different at baseline between either group, indicating a similar baseline inflammatory state (Table IV). No other significant differences were observed between TXT groups at baseline in any variables tested (Table IV).

Baseline flow cytometry values of all subjects, before ingesting $NaHCO_3$ or NaCl in solution, are presented in Table IV. Prior to any treatment, the percentages of blood leukocytes that were TNF-α^+ neutrophils, M1 macrophages, or M2 macrophages were all significantly higher in the $NaHCO_3$ TXT group when compared with baseline values obtained in the NaCl TXT group (Table IV). There was a significant TREATMENT × TIME effect on both M1 macrophages (p = 0.0004) and TNF-α–positive neutrophils (p = 0.0146), with the levels of these inflammatory cells in the plasma being reduced to a significantly greater degree following ingestion of $NaHCO_3$ when compared with NaCl (Fig. 3). The greatest decreases in blood inflammatory cells were observed at 2 and 3 h following $NaHCO_3$ ingestion. Similar to our observations in rats, oral $NaHCO_3$ ingestion increased the percentage of blood leukocytes identified by flow cytometry as M2 macrophages (p = 0.00165) (Fig. 3). Decreases in inflammatory TNF-α^+ neutrophils and M1 macrophages in the $NaHCO_3$ TXT group did not appear to be related to the differing baseline levels observed between TXT groups. When comparing individual responses between subjects of different groups, subjects with similar baseline levels of blood leukocytes responded differently if they received $NaHCO_3$ compared with NaCl (Supplemental Fig. 1).

Splenic involvement. In the current study, we found that, prior to beginning $NaHCO_3$ or vehicle treatment, either complete removal of the spleen or simple manipulation of the spleen to midline during sterile surgical laparotomy completely abolished the effect of $NaHCO_3$ to promote M1 to M2 polarization in the kidney of Dahl SS rats fed an HS diet for 2 wk (Fig. 4). Furthermore, both of these maneuvers resulted in a significant decrease in renal M2 macrophages when compared with sham laparotomy only (p = 0.02 and 0.0002, comparing laparotomy only to sham splenectomy and splenectomy for vehicle- and bicarbonate-treated groups, respectively; Fig. 4). We confirmed a functional anti-inflammatory response using the MLR. Proliferation of responder

Table III. Changes in serum electrolytes following an acute dose of $NaHCO_3$ in human subjects

	Pretreatment		Posttreatment	
	CON	TXT	CON	TXT
Na (mmol/l)	140.4 ± 0.9	141.1 ± 0.8	141.2 ± 0.4	140.8 ± 0.5
K (mmol/l)[b]	4.1 ± 0.1	4.3 ± 0.1	4.3 ± 0.1[a]	3.9 ± 0.1[a]
Cl^- (mmol/l)	100.2 ± 0.9	100.9 ± 0.9	102.4 ± 0.4	102.3 ± 0.8

All values are mean ± SE.
[a]Significant change versus baseline ($p < 0.05$).
[b]Significant group × time interaction ($p = 0.029$).

T cells isolated from the spleen of Dahl SS rats, in response to stimulation with splenocytes from $NaHCO_3$-treated rats, was significantly lower than that of control animals drinking NaCl ($n = 3$ rats each group, $p = 0.00003$; Fig. 5). In contrast to our findings in rats, in C57Blk6 mice, 3 d of oral $NaHCO_3$ (0.1 M in drinking water) increased splenic M1 macrophages and had no effect on M2 macrophages (data not shown). Further confirming the involvement of cholinergic signaling, MLA, a potent and specific inhibitor of the α7 nicotinic Ach receptor, prevented anti-inflammatory macrophage polarization to oral $NaHCO_3$ (Fig. 6). Similarly, the gastric proton pump inhibitor esomeprazole also inhibited the anti-inflammatory response to $NaHCO_3$ (Fig. 6).

Markers for M1 (Fig. 4; CD11b/80/TNF-α) and M2 (Fig. 4; CD11b/80/CD206/IL-10) macrophages were selected based on previous studies on the rat (8, 9); however, to confirm the specificity of these markers, these Abs were compared with alternative markers (CD68/CD163/CD206/TNF-α: for M1) and (CD68/CD163/CD206/IL-10: for M2). Results using both Ab markers sets were highly consistent and confirmed our observations of M1 to M2 polarization in the spleen and kidney of $NaHCO_3$-treated rats as well as the effect of splenectomy to abolish this response (Supplemental Fig. 2). In addition, we confirmed the identity of renal macrophages by specific depletion with clodronate liposomes (Supplemental Fig. 3).

Mesothelial signaling. As we found that light manipulation to visualize the spleen at midline during surgical laparotomy (sham splenectomy) was sufficient to abolish the anti-inflammatory response to oral $NaHCO_3$, we investigated how this maneuver could disrupt signaling of this response to the splenic parenchyma. Although, outside of the splenic hilum, only light connective tissue was observed to be attached to the spleen in rodents, we found that gentle splenic manipulation during surgery resulted in marked fibrosis of the splenic capsule and hypertrophy or hyperplasia of the capsular mesothelial cell layer following 2+ wk of recovery in both Sprague Dawley and Dahl SS rats (Fig. 7A). In histological sections, numerous fragile connections from the surrounding fascia were found to directly connect to the mesothelial layer along the inferior edge of the spleen (Fig. 6A). Prior to manipulation, both these connections as well as capsular mesothelial cells nearest to these junctions stained strongly positive for the pan-neuronal marker PGP9.5 as well as acetylcholine esterase, indicating cholinergic neural function (Fig. 8C, 8D, 8F, 8I). Although PGP9.5 staining within the capsular mesothelial cells was maintained following manipulation of the spleen, acetylcholine esterase staining within these now hypertrophied mesothelial cells was markedly reduced (Fig. 7D, 7E). Both acetylcholine esterase staining and tyrosine hydroxylase staining

Table IV. Baseline human subject data

Variable	Control Subjects (NaCl) $n = 6$, mean ± SE	Treatment Subjects ($NaHCO_3$) $n = 12$, mean ± SE	p (Student t Test)
Age (y)	24.8 ± 1.2	27.4 ± 2.0	NS
Height (cm)	177.0 ± 3.1	167.7 ± 3.2	NS
Weight (kg)	81.0 ± 7.8	71.9 ± 5.3	NS
BMI (kg/m^2)	25.7 ± 2.1	25.3 ± 1.2	NS
Systolic blood pressure (mmHg)	118.7 ± 4.7	118.6 ± 3.4	NS
Diastolic blood pressure (mmHg)	71.8 ± 3.2	68.3 ± 2.7	NS
CRP	1.06 ± 0.30	1.22 ± 0.58	NS
Hct (%)	45 ± 1	43 ± 2	NS
Glucose (mg/dl)	92 ± 4	90 ± 2	NS
BUN (mg/dl)	12.5 ± 1.0	13.3 ± 1.2	NS
Creatinine (mg/dl)	0.84 ± 0.06	0.85 ± 0.07	NS
Na (mM)	141 ± 1	140 ± 1	NS
K (mM)	4.0 ± 0.1	4.3 ± 0.1	NS
Cl (mM)	100 ± 1	101 ± 1	NS
CO_2 (mM)	21 ± 0	21 ± 1	NS
Protein (g/dl)	6.9 ± 0.1	6.9 ± 0.1	NS
Albumin (g/dl)	4.5 ± 0.1	4.4 ± 0.1	NS
TNF-α^+ neutrophils (% blood leukocytes)	55 ± 2.2	26 ± 7.3	0.0003*
M1 macrophages (% blood leukocytes)	3.3 ± 0.3	1.6 ± 0.5	0.007*
M2 macrophages (% blood leukocytes)	1.9 ± 0.2	1.4 ± 0.2	NS

Baseline data for subjects in $NaHCO_3$ and NaCl TXT groups. Data represent values obtained on the first day of the protocol following overnight fasting and prior to subjects ingesting either $NaHCO_3$ or NaCl solutions. Data are compared by unpaired Student t test.
*$p < 0.05$ was treated as significant.
BUN, blood urea nitrogen, CRP, C-reactive protein, Hct, hematocrit.

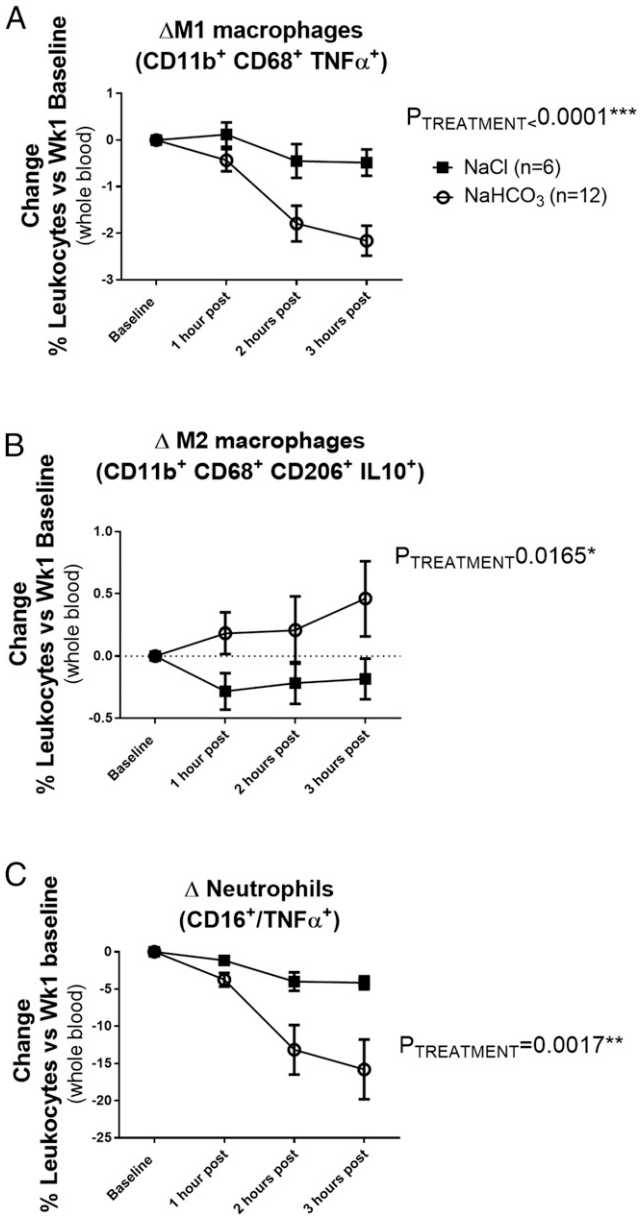

FIGURE 3. Data from flow cytometric analysis of human blood from subjects drinking either $NaHCO_3$ (bicarbonate) or equimolar NaCl (vehicle) are presented in Fig. 7A–C. *y*-axis, All data are expressed as change in the percentage of total blood leukocytes compared with baseline values taken prior to any treatment. Baseline data for all subjects are given in Table II. *x*-axis, 1 h post = data obtained 1 h after ingesting 2 g or $NaHCO_3$ ($n = 12$ subjects) or equimolar NaCl ($n = 6$ subjects) solution in 250 ml of bottled water. Two hours post = data obtained 2 h after ingesting 2 g or $NaHCO_3$ or equimolar NaCl solution in 250 ml of bottled water. Three hours post = data obtained 3 h after ingesting 2 g or $NaHCO_3$ or equimolar NaCl solution in 250 ml of bottled water (note not all subjects had blood drawn at 3 h [$n = 10$ for $NaHCO_3$ at 3 h in supplement]). All data are mean ± SE. $P_{TREATMENT}$ = the output of a two-way ANOVA comparing TXT groups. $p < 0.05$ was considered significant. (**A**) The change in percentage of total blood leukocytes identified as M1 macrophages ($CD11b^+$ $CD68^+$ TNF-α^+ cells) in vehicle- ($n = 6$; filled squares) and bicarbonate- ($n = 12$; open circles) treated subjects as compared with baseline. (**B**) The change in the percentage of total blood leukocytes identified as M2 macrophages ($CD11b^+$ $CD68^+$ $CD206^+$ IL-10^+ cells) in vehicle- ($n = 6$; filled squares) and bicarbonate- ($n = 12$; open circles)treated subjects as compared with baseline. (**C**) The change in the percentage of total blood leukocytes identified as TNF-α^+ neutrophils ($CD16^+$/TNF-α^+cells) in vehicle- ($n = 6$; filled squares) and bicarbonate- ($n = 12$; open circles) treated subjects as compared with baseline.

within the splenic parenchyma were unaffected by manipulation of the spleen (Supplemental Fig. 4). PGP9.5 and acetylcholine esterase staining was localized primarily to mesothelial cells proximal to the inferior edge of the spleen where these thin connections were present (Fig. 8G, 8I). Mesothelial cells along the superior edge of the spleen most often stained negative for these markers.

As the cholinergic anti-inflammatory pathway can be activated by vagal stimulation, and transection of the vagal nerves abolishes this response, we investigated whether vagal signaling contributed to acetylcholine esterase staining in splenic capsular mesothelial cells. Although PGP9.5 staining in mesothelial cells did not appear to be altered with vagotomy, acetylcholine esterase staining within mesothelial cell bodies on the splenic capsule was abolished with prior vagotomy, with five of five surgical control animals being found positive for mesothelial acetylcholine esterase and four out of four animals in which complete subdiaphragmatic vagotomy was confirmed, being found negative for mesothelial acetylcholine esterase staining by an observer unaware of the origin of the sections (Fig. 7F–I; $p = 0.008$).

To further investigate this phenomenon, we examined these fragile mesothelial connections to the splenic mesothelium with electron microscopy. We found that the connections contain collagen fibers lined by mesothelium on both sides (identified by their numerous microvilli), but we found no evidence of any neural tissue. Importantly, capsular mesothelial cells primarily in and around the junction of these connections were identified to contain many ultrastructural elements within their cytoplasm, which visually resembled neuronal structures. The image in Fig. 9G contains more than 15 of these pairings within the cytoplasm of the mesothelial cells pictured. These included low-density cylindrical structures that often contained a single mitochondrion, similar to the structure observed in dendrites (Fig. 9A, 9B). These dendritic structures were often adjacent to higher-density cylindrical structures, separated by an electron-dense band, similar to the arrangement of axons and dendrites in neural tissue separated by a synaptic density (Fig. 9A, 9B). No vesicular structures were identified within these "axonal" organelles. Perhaps the most remarkable structures identified were dark bands within the axonal structures that resembled synaptic ribbons (Fig. 9C, 9E), as these structures are normally only observed in nerves with rapid firing rates such as the eye and vestibular organs. To attempt to confirm the identity of these structures, we performed immunohistochemical labeling of paraffin-embedded sections of the spleen with an Ab targeted against synaptic ribbons. Immunohistochemical labeling of paraffin-embedded sections with anti-Ribeye Ab revealed positive staining of the parenchyma of the spleen. Importantly, within the capsular region, this positive staining was limited to mesothelial cells within these connections and immediately adjacent to areas where these connections made contact with the capsular surface (Fig. 9H, 9I).

While investigating the anatomical relationships of mesothelial cells on the splenic surface, using the Ca^{2+}-sensitive dye Fluo-4, we observed a dense plexus of nerves immediately below the collagen layer (Fig. 10G) of the splenic capsule. Activation of these nerves could be promoted by electrical field stimulation (Supplemental Video). Immunohistochemical analysis of transverse sections through the splenic capsule revealed that the majority of these nerves stained only lightly positive for PGP9.5 and acetylcholine esterase but were negative for tyrosine hydroxylase (Fig. 10A–F). These structures were confirmed as neurons by high-power electron microscopy imaging (Fig. 10H, 10I).

Two weeks following transection of the vagal nerves below the diaphragm in Sprague Dawley rats drinking $NaHCO_3$, splenic

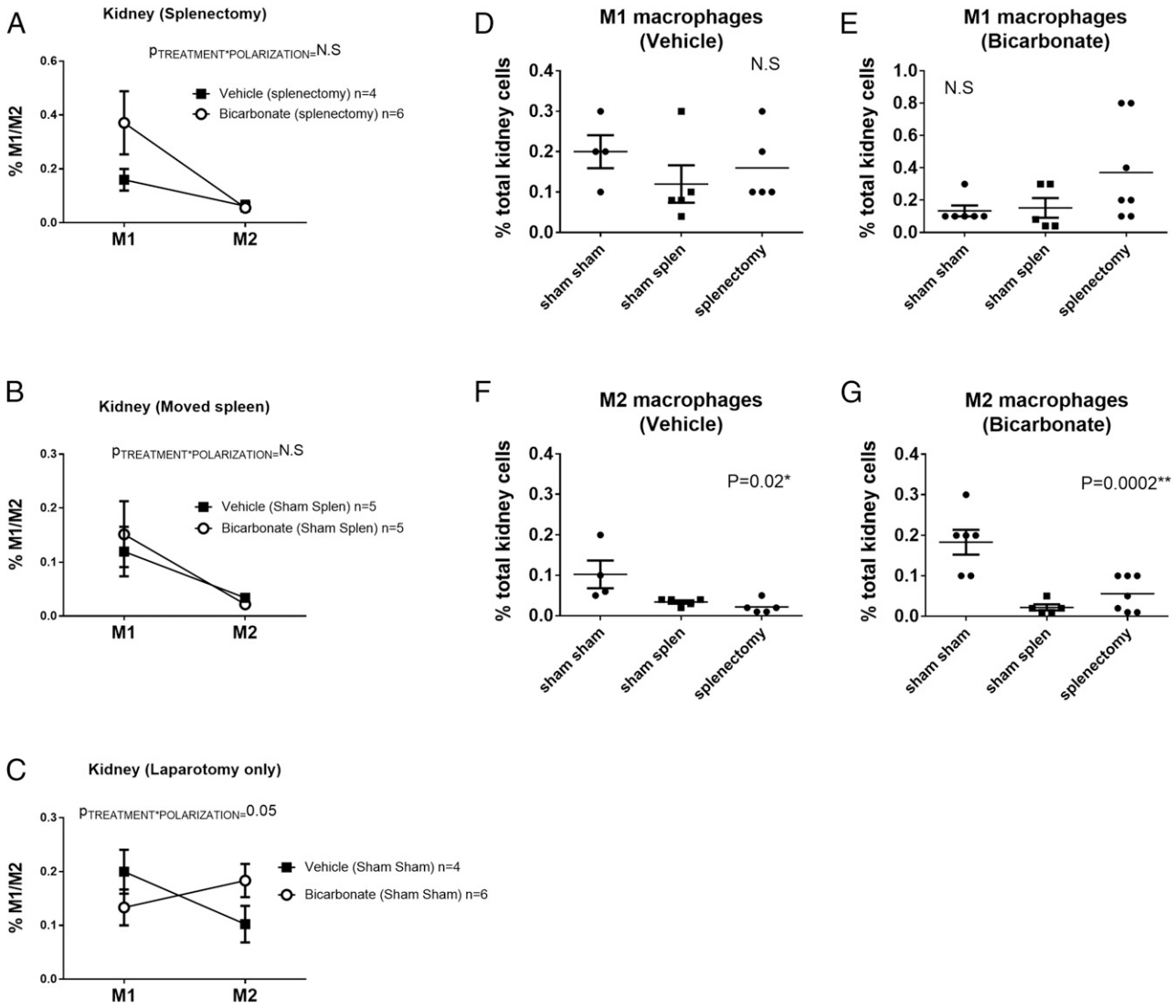

FIGURE 4. Data from flow cytometric analysis of macrophage polarization (M1/M2) from kidneys of male Dahl SS rats drinking either 0.1 M $NaHCO_3$ (bicarbonate) or equimolar NaCl (vehicle) following removal of the spleen (splenectomy) or sham splenectomy and laparotomy only (spleen not moved during surgery) are presented in Fig. 3A–G. All data are from rats placed on treated water (vehicle or bicarbonate) for 3 d before being switched to an HS diet for an additional 14 d prior to tissue harvest. (**A**) The percentage of total kidney cells identified as M1 macrophages (CD11b/F4/80$^+$/TNF-α^+ cells) and M2 macrophages (CD11b/CD206$^+$/IL10$^+$ cells) in vehicle- ($n = 4$; filled circles) and bicarbonate- ($n = 6$; filled squares) treated rats in which the spleen was removed. (**B**) The percentage of total kidney cells identified as M1 macrophages (CD11b/F4/80$^+$/TNF-α^+ cells) and M2 macrophages (CD11b/CD206$^+$/IL10$^+$ cells) in vehicle- ($n = 5$; filled circles) and bicarbonate- ($n = 5$; filled squares) treated rats in which the spleen was moved to midline during surgery but not removed (sham splenectomy). (**C**) The percentage of total kidney cells identified as M1 macrophages (CD11b/F4/80$^+$/TNF-α^+ cells) and M2 macrophages (CD206$^+$/IL10$^+$ cells) in vehicle- ($n = 5$; filled circles) and bicarbonate- ($n = 5$; filled squares) treated rats in which the spleen was untouched during surgery (Sham Sham). (**D**) The percentage of total renal cells identified as M1 macrophages (CD11b/F4/80$^+$/TNF-α^+ cells) in vehicle-treated rats in which the spleen was removed (splenectomy), moved but not removed (sham spleen), and left untouched (Sham Sham) ~28 d prior to tissue harvest. Individual animal data are shown (circles) with mean and SE. (**E**) The percentage of total renal cells identified as M1 macrophages (F4/80$^+$/TNF-α^+ cells) in bicarbonate-treated rats in which the spleen was removed (splenectomy), moved but not removed (sham spleen), and left untouched (Sham Sham) ~28 d prior to tissue harvest. Individual animal data are shown (circles) with mean and SE. (**F**) The percentage of total renal cells identified as M2 macrophages (CD206$^+$/IL10$^+$ cells) in vehicle-treated rats in which the spleen was removed (splenectomy), moved but not removed (sham spleen), and left untouched (Sham Sham) ~28 d prior to tissue harvest. Individual animal data are shown (circles) with mean and SE. (**G**) The percentage of total renal cells identified as M2 macrophages (CD206$^+$/IL10$^+$ cells) in bicarbonate-treated rats in which the spleen was removed (splenectomy), moved but not removed (sham spleen), and left untouched (Sham Sham) ~28 d prior to tissue harvest. Individual animal data are shown (circles) with mean and SE.

weight was reduced in vagotomized animals (0.92 ± 0.05 g) when compared with surgical control animals (1.29 ± 0.04 g; $p < 0.0001$), with spleens accounting for 0.28 ± 0.01% and 0.35 ± 0.01% ($p < 0.01$) of total body weight in vagal denervated and control animals, respectively. In rats in which these connections had been disrupted, vagotomy had no further effect to reduce spleen weight, indicating that both maneuvers likely cause regression of the splenic parenchyma through a common pathway (Fig. 11).

Discussion

The first major finding of our study is that oral $NaHCO_3$ promotes a powerful anti-inflammatory response including M1 to M2 macrophage polarization and increased FOXP3$^+$ CD4$^+$ T regulatory

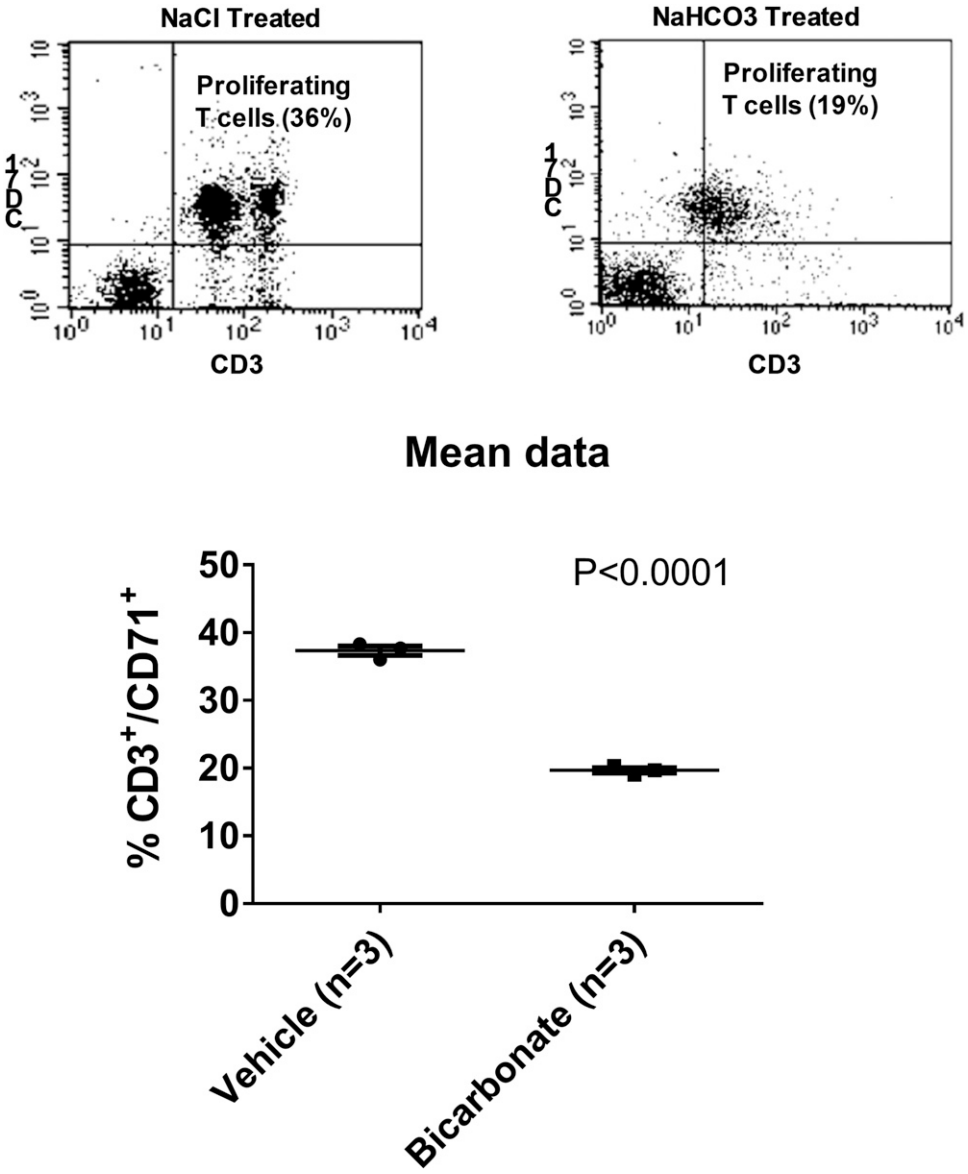

FIGURE 5. MLR. Top, Representative flow cytometry dotplots depict cellular proliferation of T cells after 96 h of incubation with mixed splenocytes from animals either treated with oral NaCl (left, 0.1 M for 3 d) or $NaHCO_3$ (right, 0.1 M for 3 d). *x*-axis, $CD71^+$ cells. *y*-axis, $CD3^+$ cells. Mean data ± SE as well as individual animal data (circles; $n = 3$ for each TXT group), are shown in the lower panel. P = result of unpaired *t* test.

cells (Tregs) within the spleen. We confirmed that these phenotypic changes were associated with functional anti-inflammatory effects using the MLR. As the Dahl SS rat model develops hypertension and renal injury when fed an HS diet, to determine whether $NaHCO_3$ promotes an anti-inflammatory phenotype independent of these changes, we examined tissues from LS-fed Dahl rats and normotensive Sprague Dawley rats. Our data indicate that the effect of $NaHCO_3$ on macrophage polarization was independent of salt diet or elevated blood pressure. In agreement with our findings in rats, oral $NaHCO_3$ promoted a robust anti-inflammatory response in the blood of subjects (Fig. 3), which was evident in as little as 1 h after ingestion. To our knowledge, these data are the first demonstration that orally ingested $NaHCO_3$ can promote a powerful anti-inflammatory response in both rats and humans.

We speculate that the anti-inflammatory effects of oral $NaHCO_3$ ingestion are mediated by activation of the cholinergic anti-inflammatory pathway. The cholinergic anti-inflammatory pathway has been reported to be the efferent arm of the anti-inflammatory reflex (15), which acts via vagal efferents to promote M2 macrophage polarization in the spleen and limit activation of the innate immune system, thereby preventing damage caused by excessive cytokine production (4, 16). Inflammatory macrophages and excessive TNF-α production have been implicated in the pathology of a broad range of disease states, including rheumatoid arthritis (17), cardiovascular disease (18), atherosclerosis (19, 20), irritable bowel disease (21), type 2 diabetes (22), and neurodegenerative diseases as well as others (23–26). Conversely, $FOXP3^+$ Tregs have been shown to be beneficial in a wide range of pathologies. $FOXP3^+$ Tregs act to suppress activation of the immune system and induce immune tolerance (27). Evidence suggests that expansion of Tregs may be beneficial in a wide variety of disease states that involve pathological activation of the immune system, including allergy (28), asthma (28), multiple sclerosis (29), graft versus host disease (30), diabetes (31), and hypertension (32, 33) as well as many others. Given its therapeutic potential against inflammatory disease, there is currently much interest in methods to activate the cholinergic anti-inflammatory

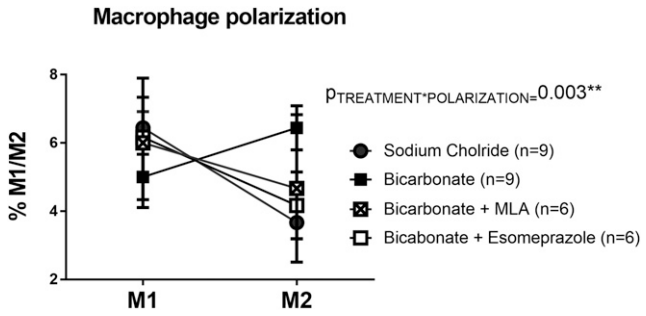

FIGURE 6. Data from flow cytometric analysis of macrophage polarization (M1/M2) from spleens of male Sprague Dawley rats drinking either 0.1 M $NaHCO_3$ (bicarbonate; filled squares; $n = 9$) or equimolar NaCl (vehicle; filled circles; $n = 9$) or bicarbonate with inhibition with MLA (5 mg/kg; Sigma; bicarbonate + MLA; crossed squares; $n = 6$) and bicarbonate + esomeprazole (20 mg/kg; Sigma; empty squares; $n = 6$). All data are from rats placed on treated water (vehicle or bicarbonate) for 3 d. *y*-axis, The percentage of total kidney cells identified as M1 macrophages (CD68+/CD163+/CD206−/TNF-α+ cells) and M2 macrophages (CD68+/CD163+/CD206+/IL-10+ cells). $P_{TREATMENT*POLARIZATION}$ = the output of a two-way ANOVA comparing all TXT groups. $p < 0.05$ was considered significant.

pathway. Activation of vagal efferents by noninvasive ultrasound has been demonstrated to reduce kidney injury following ischemia reperfusion (34). Furthermore, in humans, efforts to stimulate the cholinergic anti-inflammatory pathway chronically by implanting stimulating electrodes on the vagal nerves have shown promise in patients with rheumatoid arthritis (17). Consistent with activation of the cholinergic anti-inflammatory pathway, in rats, removal of the spleen or treatment with the α7 nicotinic Ach receptor antagonist MLA abolished the anti-inflammatory effect of oral $NaHCO_3$ intake. Our data indicate that oral $NaHCO_3$ loading may provide a cheap, relatively safe, effective, and easily accessible and/or noninvasive method to activate cholinergic anti-inflammatory pathways in humans, which may be of benefit to patients suffering from a multitude of inflammatory disease states. As such, our findings could potentially have significant clinical application to the treatment of human disease. Future studies testing the efficacy of oral $NaHCO_3$ to limit injury in models of inflammatory disease will be required to determine the therapeutic potential of this stimuli.

Our initial interest in oral $NaHCO_3$ was in relation to its protective effect against kidney functional decline. By limiting the ability of the kidneys to excrete an acid load, loss of kidney parenchyma in CKD patients can promote metabolic acidosis (35). Oral $NaHCO_3$ was first given to CKD patients to prevent the deleterious effects of metabolic acidosis on nonrenal functions; however, evidence from a number of small clinical trials as well as experimental models now indicates that oral $NaHCO_3$ supplementation may also slow the decline in kidney function in CKD patients, even in the absence of metabolic acidosis (6). As chronic inflammation has been implicated in both acute and chronic kidney injury (1–3), we investigated the effect of oral $NaHCO_3$ on inflammatory cell profiles within the kidney. Our finding that oral $NaHCO_3$ promotes anti-inflammatory immune polarization is consistent with the hypothesis that oral $NaHCO_3$ may protect the kidney, at least in part, by activating a cholinergic anti-inflammatory pathway. In the current study we did not maintain animals on oral $NaHCO_3$ long enough to determine if there were differences in the rate of glomerular filtration rate (GFR) decline. This experiment is particularly difficult in the Dahl SS rat model as these rats develop malignant hypertension when fed salt in the drinking water, which causes them to die prematurely of stroke, often before major reductions in GFR are observed. As such, long-term studies in a normotensive model of CKD may be required to determine whether the anti-inflammatory effects of $NaHCO_3$ administration contribute to maintenance of GFR in the rat. Interestingly, we found that inhibition of gastric proton pumps prevented oral $NaHCO_3$ from activating an anti-inflammatory response, suggesting that gastric H^+ secretion is required. This finding may be particularly relevant to CKD, as long-term use of proton pump inhibitors has been associated with increased risk of developing CKD (36).

There has been much debate in regards to the mechanisms through which efferent cholinergic signals from the vagal nerves are transmitted to the spleen (37–39). At the heart of this debate is the apparent lack of vagal innervation to the spleen. Although some studies have reported evidence of vagal innervation at the splenic poles in rodents (38), this remains controversial, and most current reports favor a mechanism in which efferent vagal signals are transmitted to the spleen via sympathetic nerves [this hypothesis, however, has also been refuted (40)], which enter along the vessels of the splenic plexus and/or via nonneuronal acetylcholine signaling initiated by circulating T cells that receive vagal input outside of the splenic parenchyma (41, 42). Both of these pathways are thought to result in activation of α-7–containing nicotinic receptors on splenic macrophages. Acetylcholine is synthesized in practically all living cells (43), and many components of acetyl-choline signaling have been found in mesothelial cells of the lung (44) and intestine (45). In addition to a barrier function, mesothelial cells have been reported to express TLR (46), act as APC (47), and are known to produce a number of immunoregulatory factors including COX2, iNOS, IL-1B, TNF-α, and MCP-1 (45). Taken together, our data indicate a previously unrecognized function of the mesothelium to mediate splenic anti-inflammatory responses via cholinergic signaling to the splenic capsule. Such a mechanism may resolve much of the current controversy regarding how vagal stimulation alters splenic function, suggesting cholinergic signals may be transmitted to the splenic capsule not by vagal efferent nerves but by the mesothelium. Our findings are consistent with a recent report by Mihara et al. (45) who found that stimulation of the α-7 nicotinic acetylcholine receptor on rat intestinal mesothelial cells blunted the inflammatory response of these cells to LPS. Interestingly, these investigators also reported that enteric nerves (presumed to be vagal efferents) adhered to the mesothelial cells of the ileal serosa, leading the authors to speculate that the anti-inflammatory effects of the mesothelium in the ileum may be stimulated by autonomic nerves (45). To our knowledge, our data are the first evidence that mesothelial cells may have a "neuronal-like" function innervating the splenic capsule. Although our histological findings provide an explanation for our immunological data, our finding of neuronal-like function in mesothelial cells is unprecedented and raises a number of important questions. Although we are unable to address these questions in the current study, further studies are warranted, as similar innervation by mesothelial cells in other organs could represent a previously unrecognized pathway of biological communication.

Our finding that PGP9.5 staining within the capsular mesothelial cells was maintained, and that following transection of the vagal nerves, these cells did not hypertrophy as they did following movement of the spleen indicates that these cells maintained a "neural phenotype" in the absence of vagal input. These findings raise the possibility that these cells may receive signals from sources other than the vagal nerves. Evidence for vagal regulation of immunity derives from observations that vagal stimulation promotes an anti-inflammatory response that originates in the spleen (48). Given that there is no known vagal innervation to the spleen,

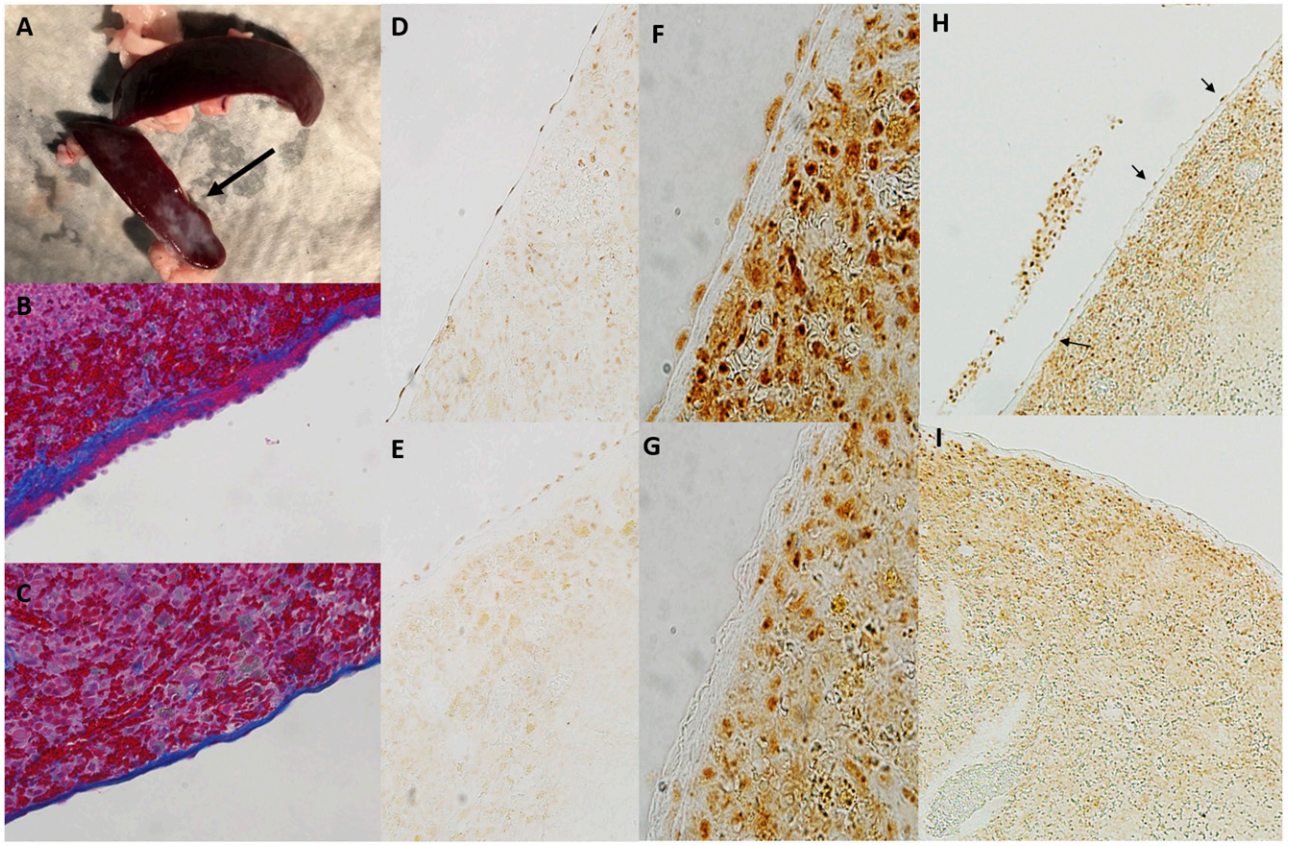

FIGURE 7. Effect of splenic movement or vagal denervation on the splenic mesothelium. (**A**) Shown is a spleen harvested from a surgical control rat (top, laparotomy only) and rat in which the spleen was moved to midline during surgery. Surgery was performed on both rats 28 d prior to tissue harvest. Fibrosis of parts of the splenic capsule (arrow) can be observed in spleens harvested from rats in which the spleen was manipulated to midline during surgery. (**B**) Shown is trichrome-stained image of the splenic capsule (original magnification ×20) demonstrating thickening on the capsule (blue staining) and mesothelial cell hypertrophy and hyperplasia (pink on capsule) typical of a spleen that has been manipulated to midline during surgical laparotomy. (**C**) Shown is normal capsule histology (original magnification ×20) in a surgical sham rat in which the spleen was not moved (trichrome staining). Note the thin capsule and flattened mesothelial cell layer when compared with the image shown in (B). (**D**) Acetylcholine esterase staining of capsular mesothelial cells in a surgical sham rat. Note the flattened appearance of the mesothelial cells and strong positive staining for acetylcholine esterase (original magnification ×20). (**E**) Acetylcholine esterase staining of capsular mesothelial cells in a rat in which the spleen had been moved to midline during surgery. Note the thickened capsular layer and hypertrophied appearance of the mesothelial cells. Positive staining for acetylcholine esterase is present but markedly less than that observed in control tissue (original magnification ×20). (**F**) Acetylcholine esterase staining of capsular mesothelial cells in a surgical sham rat in which the esophagus was visualized but the vagal nerves left untouched without moving the spleen. Note the flattened appearance of the mesothelial cells and strong positive staining for acetylcholine esterase (original magnification ×40). (**G**) Acetylcholine esterase staining of capsular mesothelial cells in a rat in which the vagal nerves were transected below the diaphragm without moving the spleen 14 d prior to tissue harvest. Note the absence of positive staining for acetylcholine esterase specifically in the surface mesothelial layer (original magnification ×40). (**H**) Low-power image of spleen described in (F). Mesothelial cells staining positive for acetylcholine esterase can be observed as a necklace-like appearance along the splenic capsule (indicated by arrows) (original magnification ×10). (**I**) Low-power image of spleen described in (G). Note the lack of positive-stained mesothelial cells on the splenic capsule. Acetylcholine esterase staining remains similar to control tissue in all other regions of the splenic parenchyma. Cells within and immediately below the capsule continue to stain positive for acetylcholine esterase (original magnification ×10).

selective vagal denervation of the spleen has been impossible. Consequently, studies aimed at demonstrating the role of the vagal nerves in the splenic anti-inflammatory response have either also stimulated or also inhibited vagal signaling to the gastrointestinal tract (15, 49–52). Our data indicating that oral ingestion of $NaHCO_3$ promotes an anti-inflammatory response, which is inhibited by an antagonist of the gastric proton pump, raises the possibility that the effect of vagal stimulation or denervation to promote or inhibit the anti-inflammatory response, respectively, is secondary to the common denominator between these stimuli: the stimulation of acid secretion in the stomach (53–55). This hypothesis is consistent with findings that Ghrelin, which also stimulates acid secretion, can activate the anti-inflammatory pathway (56). Our finding that mesothelial cells are required to mediate this anti-inflammatory response provides a potential sensory mechanism for this alternative hypothesis, whereby stomach acid secretion alters some factor within the peritoneal milieu, such as pH, that is sensed by the mesothelium that lines this compartment. Such a mechanism may be of physiological importance in deciphering whether Ags absorbed by the gut are inert (coming after a meal) or represent a potential infection of the peritoneum with ensuing acid production by invading bacteria and providing the appropriate response, either tolerance or inflammatory immune response, respectively. This alternative hypothesis challenges our current understanding of how vagal nerve stimulation promotes the cholinergic anti-inflammatory response in the spleen, suggesting for the first time that there may be no direct interface between the nervous and immune systems. In light of our data, further studies are warranted to determine whether promotion of an anti-inflammatory effect following stimulation of vagal nerves (classical activation of the cholinergic anti-inflammatory response) occurs independent of a requirement to stimulate stomach acid secretion.

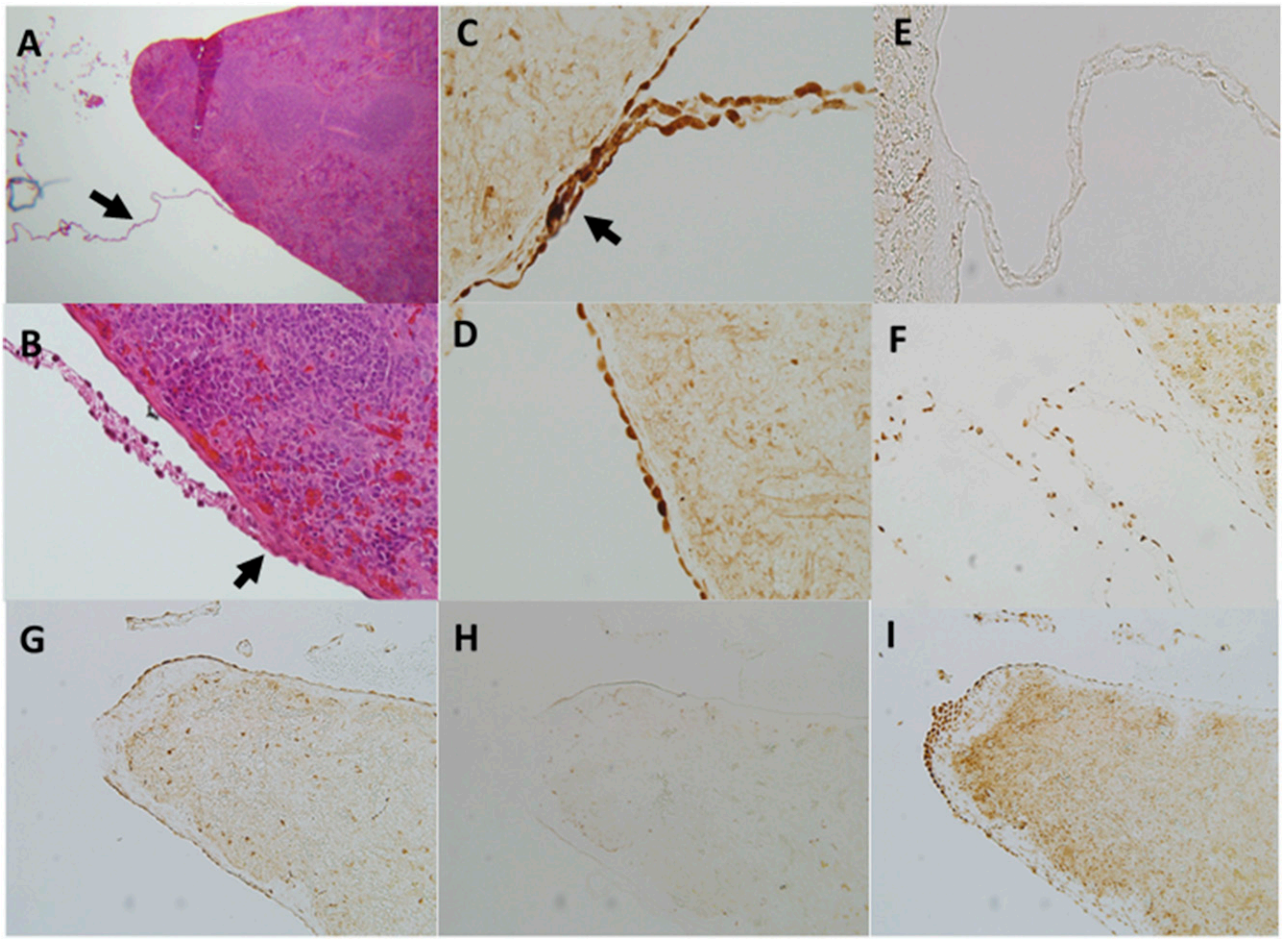

FIGURE 8. Evidence of neuronal connections to the splenic mesothelium. (**A**) Thin connections to the splenic capsule can be observed in trichrome-stained rat spleens at low power (original magnification ×5) that are not observed by the naked eye (arrow). The origin of these connections is uncertain, but they appear to be common at the splenic poles and along the inferior edge of the spleen surface. (**B**) A connection (arrow) at higher magnification (original magnification ×40). Trichrome-stained tissue connects on the capsular surface often forming a "raised nodule," which protrudes from the capsule more than the surrounding mesothelial layer. (**C**) These connections stain strongly positive for the pan-neuronal marker PGP9.5. Shown is a connection (arrow) from a control rat stained for PGP9.5. Note also the positive staining on the surrounding mesothelial layer. This was present only on the inferior axis of the spleen and was most evident in areas where connections such as this were observed (original magnification ×40). (**D**) PGP9.5 staining of capsular mesothelial cells in a surgical sham rat. Note the flattened appearance of the mesothelial cells and strong positive staining for PGP9.5 (original magnification ×40). (**E**) These connections stain negative for the sympathetic neuronal marker tyrosine hydroxylase. Note strong positive staining was observed around blood vessels in the splenic parenchyma (one can be observed directly below the intersection point of this connection) (original magnification ×20). (**F**) Acetylcholine esterase staining within a connection to the splenic capsule in a control rat. Note punctate positive staining for acetylcholine esterase throughout the connection. Positive staining for acetylcholine esterase can also be observed in the surrounding capsular mesothelial cells and underlying splenic parenchyma (original magnification ×40). (**G**) PGP9.5 staining at the inferior edge of the spleen. Mesothelial cells in this region stain strongly positive for the pan-neuronal marker PGP9.5 (original magnification ×5). (**H**) Tyrosine hydroxylase staining at the inferior edge of the spleen. Mesothelial cells in this region stain negative for the sympathetic neuronal marker tyrosine hydroxylase (original magnification ×5). (**I**) Acetylcholine esterase staining at the inferior edge of the spleen. Mesothelial cells in this region stain strongly positive for the parasympathetic neuronal marker acetylcholine esterase (original magnification ×5).

A number of previous studies have investigated potential cholinergic innervation of the spleen and found no evidence of significant innervation (37). For example, Bellinger et al. (57) found little effect of vagal transection on acetylcholine esterase staining or choline acetyltransferase activity in the spleen of adult rats. How then can we reconcile our data with the results of these previous studies? One possibility that may explain our differing findings is that mesothelial cells represent a small fraction of total splenic tissue and thus would be unlikely to contribute significantly to total splenic choline acetyltransferase activity. Furthermore, as discussed below, the mesothelial cells themselves may not be directly responsible for signaling immune cells within the splenic tissue, lessening the need for significant parenchymal innervation (57). In difference to previous reports, our immunohistochemical studies were focused on the splenic mesothelium. As mesothelial cells reside on the splenic surface and Abs can often accumulate around the edge of the tissue, it is possible that previous investigators disregarded positive staining for acetylcholine esterase in these cells as nonspecific. Our observation that only mesothelial cells along the inferior axis of the splenic capsule stain positive for acetylcholine esterase, as well as evidence that this staining is lost following transection of the vagal nerves, however, strongly refute this possibility. Furthermore, these same cells stain positive for the pan-neuronal marker PGP9.5. It is also possible that mesothelial staining was simply missed by previous investigators. In this regard, unless specifically focusing on the mesothelial layer on the inferior axis of the splenic

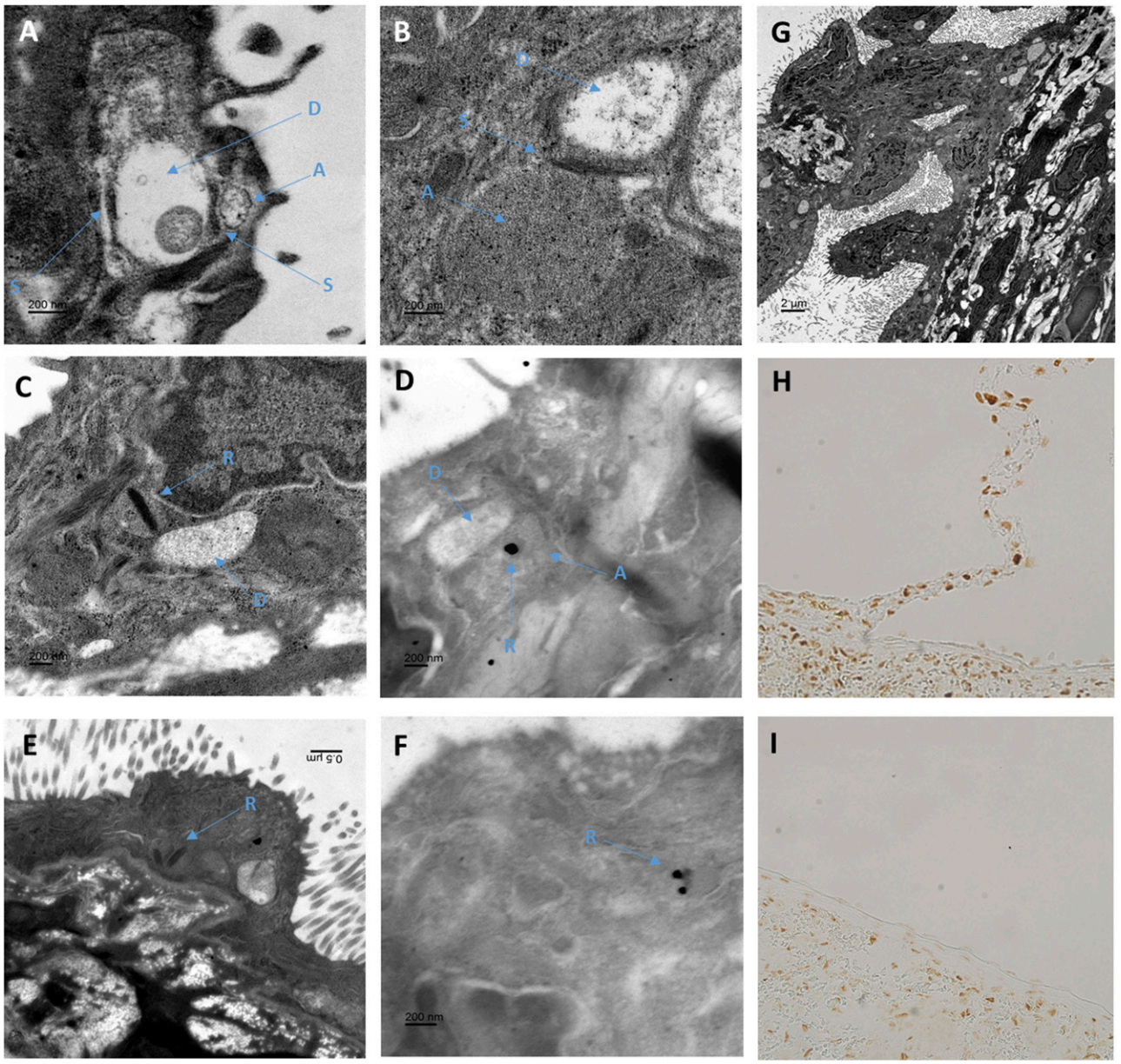

FIGURE 9. Neuronal-like structures identified within mesothelial cells connecting to the splenic capsule. (**A** and **B**) Osmium-stained electron micrographs of mesothelial cells on the inferior edge of a Sprague Dawley rat splenic capsule located close to the branch point of a connection. Mesothelial cells were identified by their location above the collagen layer of the splenic capsule and their numerous microvilli. Structures within the mesothelial cell cytoplasm resemble similar structures fond in neuronal tissue. In these images, electron-dense structures similar to that of synaptic junctions (S) can be observed between two circular structures. In (A), one of these low-density circular structures contains a single mitochondrion. These structures are similar to that observed in dendrites (D) of neuronal cells. More densely filled structures run adjacent to the dendritic structure separated by (S), which resemble axons (A) in their arrangement with the dendritic structures and greater electron density. No clear vesicular structures were observed within (A). (**C** and **E**) Many of the "axonal-looking" structures (A) were found to contain a dense elongated core, similar to synaptic ribbons (R) observed in the axons of rapidly firing neural cells. (**D** and **F**) Shown are urethane-stained sections, which provide less ultrastructural contrast but allow Ag-specific staining. Immunogold labeling of Abs against ribeye, a core component of synaptic ribbons, demonstrated gold particle deposition on the dark-banded structures within mesothelial cells that resembled synaptic ribbons (R). (**G**) In this low-magnification osmium-stained section, a tissue connection with the splenic capsule can be observed. Mesothelial cells, identified by their microvilli, can be seen lining the entire length of the connection before making contact with other mesothelial cells on the splenic surface. At higher magnification, >15 object pairs, similar to that observed in (C and D), containing all of axon- (A), ribbon- (R), and dendritic- (D) like structures can be seen in this image. (**H** and **I**) Paraffin-embedded sections of rat spleen stained with anti-ribeye, a core component of synaptic ribbons. As shown in (H), mesothelial cells located on structures that connect to the splenic capsule as well as mesothelial cells immediately adjacent to these junctions stain positive for ribeye. As demonstrated in (I), mesothelial cells in areas where these junctions are not present are negative for ribeye, whereas the splenic parenchyma is positive.

capsule, our own observations indicate there is little difference in acetylcholine esterase staining following vagal transection in other regions of the spleen.

One question raised by our data is, "How can mesothelial cells alter the immune cell profile within the spleen?" Perhaps mesothelial cells directly secrete acetyl-choline onto the splenic capsule, altering local splenic monocyte or T cell activation state. Alternatively, mesothelial cells could act via a more complex signaling process. In this regard, it is interesting that we observe a dense network of nerves directly below the splenic capsule on

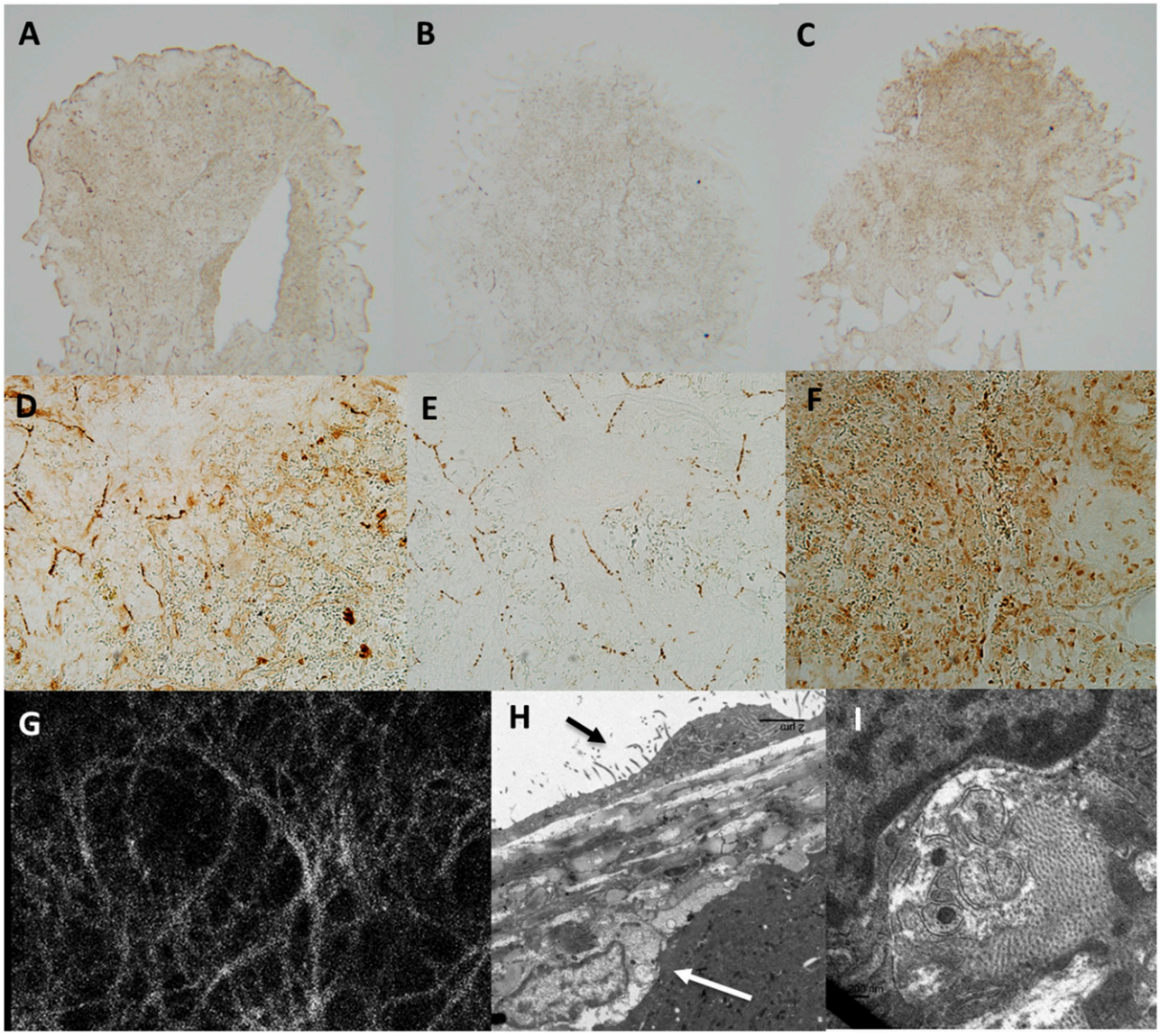

FIGURE 10. Dense network of acetylcholine esterase–positive nerves immediately below the splenic capsule. (**A** and **D**) Thin (5 mm) sections through the frontal plane of the splenic capsule indicate strong and diffuse positive staining for the pan-neuronal marker PGP9.5 in the capsular layer. (A) Original magnification ×5. (D) Original magnification ×20. (**B** and **E**) Thin (5 mm) sections through the frontal plane of the splenic capsule indicate strong positive staining for the sympathetic neuronal marker tyrosine hydroxylase in the capsular layer, with tyrosine hydroxylase–positive tissue forming a lose web of interconnected nerves. (B) Original magnification ×5. (E) Original magnification ×20. (**C** and **F**) Thin (5 mm) sections through the frontal plane of the splenic capsule indicate strong and diffuse positive staining for the parasympathetic neuronal marker acetylcholine esterase in the capsular layer. (C) Original magnification ×5. (F) Original magnification ×20. (**G**) The splenic capsule viewed at 40× on a confocal microscope. Tissue was loaded with the Ca^{2+}-sensitive indicator fluo-4. Note a dense layer of nerve tissue can be observed directly below the mesothelial cell layer across the entire splenic capsule. The density of this neural web is much greater than that observed in (B) and (E) in tissue stained positive for tyrosine hydroxylase, indicating additional nerve tissue is present. Activation of these nerves can be stimulated by electrical field stimulation (see supplement). (**H**) Transmission electron microscopy indicates that nerves sit directly below the splenic capsule. Black arrow indicates capsular mesothelial cell. White arrow indicates nerve closely associated with the splenic capsule. Bar, 5 μm. (**I**) Nerves are identified by the presence of intracellular vesicles typical of synaptic junctions.

which the mesothelial cells reside (Fig. 10, Supplemental Video). Although it has been previously reported that the splenic capsule is innervated, this innervation was reported to consist primarily of tyrosine hydroxylase–positive sympathetic nerves that arise from blood vessels that supply the splenic parenchyma (58). In difference, we find that the majority of capsular nerves stain negative for tyrosine hydroxylase and instead stain lightly positive for acetylcholine esterase and PGP9.5. Importantly, and consistent with previous reports, acetylcholinesterase staining was not altered in this region of the spleen following either manipulation of the spleen or subdiaphragmatic vagal denervation, suggesting these nerves are not of vagal origin (57). Given their close anatomical arrangement, we speculate that mesothelial cells may release paracrine factors, such as acetylcholine, that alter the signaling of these capsular ([perhaps sympathetic (57)]) nerves, which may then modulate the anti-inflammatory response within the splenic parenchyma. Such a signaling pathway could potentially explain why sympathetic denervation of the spleen results in loss of cholinergic anti-inflammatory responses, as sympathetic denervation has been demonstrated to abolish acetylcholinesterase staining in the region in which these underlying nerves are located (57). Importantly, we found no evidence that simple manipulation of the spleen altered

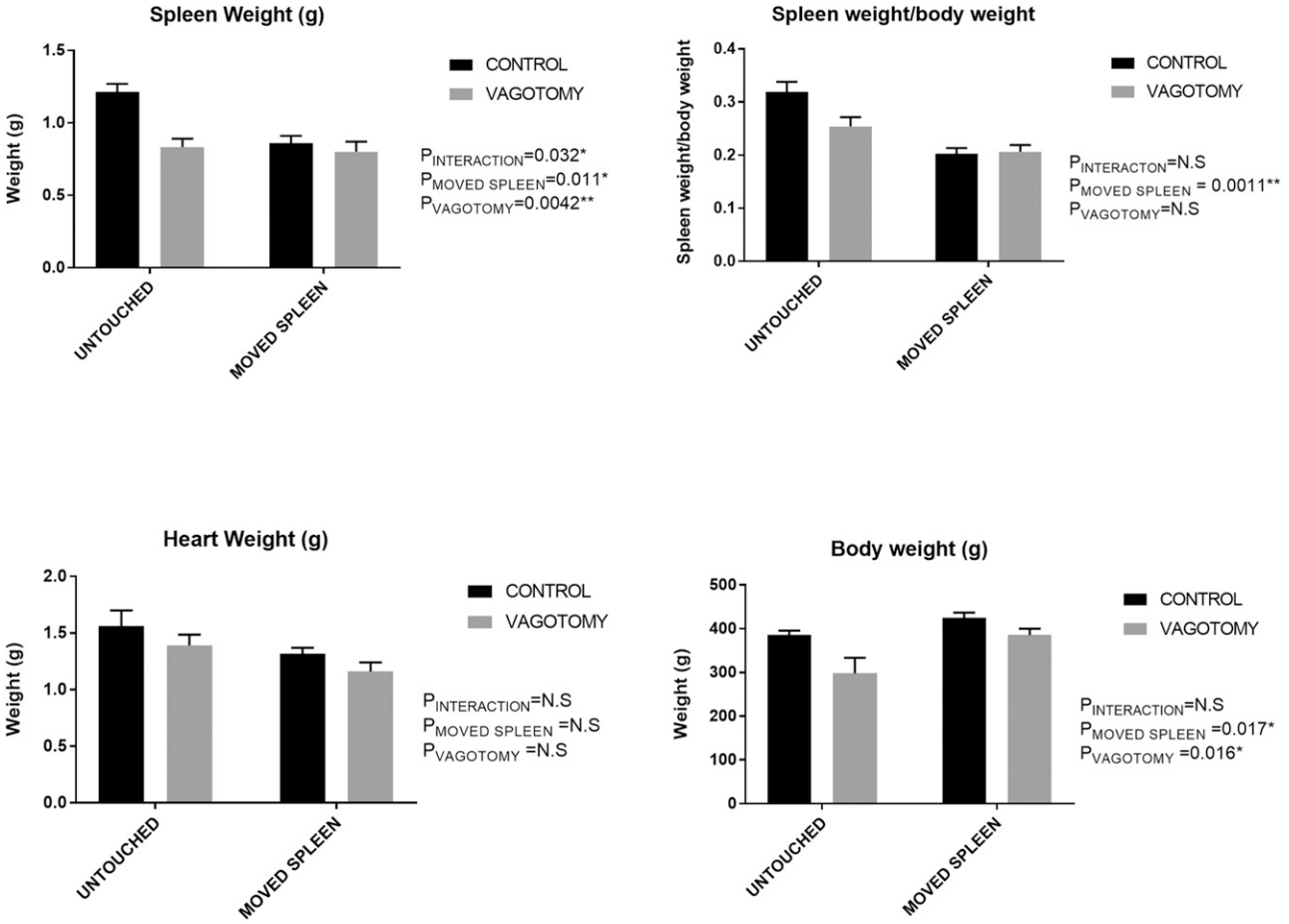

FIGURE 11. Tissue weights 2 wk following surgery in Sprague Dawley rats. Data are mean ± SE. p values represent results of two-way ANOVA comparing groups as indicated. $p < 0.05$ was considered significant. n = 15/9/5/5 for untouched control, untouched vagotomy, moved spleen control, and moved spleen vagotomy groups, respectively.

sympathetic innervation of the spleen, as indicated by tyrosine hydroxylase staining (Supplemental Fig. 4).

In summary, we report that oral $NaHCO_3$ activates splenic anti-inflammatory pathways in both rats and humans. Our novel finding provides a potentially practical and/or cost-effective and relatively safe method to activate splenic anti-inflammatory pathways in humans and therefore may have significant therapeutic potential for inflammatory disease. We provide both functional (flow cytometry) and anatomical and histological evidence that the signals that mediate this response are transmitted to the spleen via a novel neuronal-like function of mesothelial cells. To our knowledge, this is the first evidence that mesothelial cells may have a role in transmitting cholinergic signals to distal sites and, combined with evidence that gastric acid secretion is required to promote an anti-inflammatory response to $NaHCO_3$, raises the possibility that there may be no direct interface between the nervous and immune systems. Future studies testing the efficacy of oral $NaHCO_3$ to limit injury in models of inflammatory disease will be required to determine the therapeutic potential of this stimuli.

Acknowledgments

We thank the Augusta University Histology Core for help with sample preparation and analysis.

Disclosures

The authors have no financial conflicts of interest.

References

1. Cao, Q., D. C. Harris, and Y. Wang. 2015. Macrophages in kidney injury, inflammation, and fibrosis. *Physiology (Bethesda)* 30: 183–194.
2. Amdur, R. L., H. I. Feldman, J. Gupta, W. Yang, P. Kanetsky, M. Shlipak, M. Rahman, J. P. Lash, R. R. Townsend, A. Ojo, et al; CRIC Study Investigators. 2016. Inflammation and progression of CKD: the CRIC study. *Clin. J. Am. Soc. Nephrol.* 11: 1546–1556.
3. Kim, H. W., C. K. Lee, H. S. Cha, J. Y. Choe, E. J. Park, and J. Kim. 2015. Effect of anti-tumor necrosis factor alpha treatment of rheumatoid arthritis and chronic kidney disease. *Rheumatol. Int.* 35: 727–734.
4. Tracey, K. J. 2002. The inflammatory reflex. *Nature* 420: 853–859.
5. Inoue, T., C. Abe, S. S. Sung, S. Moscalu, J. Jankowski, L. Huang, H. Ye, D. L. Rosin, P. G. Guyenet, and M. D. Okusa. 2016. Vagus nerve stimulation mediates protection from kidney ischemia-reperfusion injury through α7nAChR + splenocytes. *J. Clin. Invest.* 126: 1939–1952.
6. Łoniewski, I., and D. E. Wesson. 2014. Bicarbonate therapy for prevention of chronic kidney disease progression. *Kidney Int.* 85: 529–535.
7. De Miguel, C., N. P. Rudemiller, J. M. Abais, and D. L. Mattson. 2015. Inflammation and hypertension: new understandings and potential therapeutic targets. *Curr. Hypertens. Rep.* 17: 507.
8. Li, X., M. Yang, Z. Li, M. Xue, Z. Shangguan, Z. Ou, M. Liu, S. Liu, S. Yang, and X. Li. 2016. Fructus xanthii improves lipid homeostasis in the epididymal adipose tissue of rats fed a high-fat diet. *Mol. Med. Rep.* 13: 787–795.
9. Crissey, J. M., J. Padilla, V. J. Vieira-Potter, P. K. Thorne, L. G. Koch, S. L. Britton, J. P. Thyfault, and M. H. Laughlin. 2015. Divergent role of nitric oxide in insulin-stimulated aortic vasorelaxation between low- and high-intrinsic aerobic capacity rats. *Physiol. Rep.* 3: e12459.
10. Kim, K. J., and J. A. Filosa. 2012. Advanced in vitro approach to study neurovascular coupling mechanisms in the brain microcirculation. *J. Physiol.* 590: 1757–1770.
11. Baban, B., P. R. Chandler, B. A. Johnson, III, L. Huang, M. Li, M. L. Sharpe, L. M. Francisco, A. H. Sharpe, B. R. Blazar, D. H. Munn, and A. L. Mellor. 2011. Physiologic control of IDO competence in splenic dendritic cells. *J. Immunol.* 187: 2329–2335.
12. Baban, B., P. R. Chandler, M. D. Sharma, J. Pihkala, P. A. Koni, D. H. Munn, and A. L. Mellor. 2009. IDO activates regulatory T cells and blocks their conversion into Th17-like T cells. *J. Immunol.* 183: 2475–2483.

13. Braun, M., K. Vaibhav, N. Saad, S. Fatima, D. W. Brann, J. R. Vender, L. P. Wang, M. N. Hoda, B. Baban, and K. M. Dhandapani. 2017. Activation of myeloid TLR4 mediates T lymphocyte polarization after traumatic brain injury. *J. Immunol.* 198: 3615–3626.
14. Jin, C., J. Sun, C. A. Stilphen, S. M. Smith, H. Ocasio, B. Bermingham, S. Darji, A. Guha, R. Patel, A. M. Geurts, et al. 2014. HV1 acts as a sodium sensor and promotes superoxide production in medullary thick ascending limb of Dahl salt-sensitive rats. *Hypertension* 64: 541–550.
15. Rosas-Ballina, M., and K. J. Tracey. 2009. Cholinergic control of inflammation. *J. Intern. Med.* 265: 663–679.
16. Tracey, K. J. 2009. Reflex control of immunity. *Nat. Rev. Immunol.* 9: 418–428.
17. Koopman, F. A., S. S. Chavan, S. Miljko, S. Grazio, S. Sokolovic, P. R. Schuurman, A. D. Mehta, Y. A. Levine, M. Faltys, R. Zitnik, et al. 2016. Vagus nerve stimulation inhibits cytokine production and attenuates disease severity in rheumatoid arthritis. *Proc. Natl. Acad. Sci. USA* 113: 8284–8289.
18. Kain, D., U. Amit, C. Yagil, N. Landa, N. Naftali-Shani, N. Molotski, V. Aviv, M. S. Feinberg, O. Goitein, T. Kushnir, et al. 2016. Macrophages dictate the progression and manifestation of hypertensive heart disease. *Int. J. Cardiol.* 203: 381–395.
19. Colin, S., G. Chinetti-Gbaguidi, and B. Staels. 2014. Macrophage phenotypes in atherosclerosis. *Immunol. Rev.* 262: 153–166.
20. De Paoli, F., B. Staels, and G. Chinetti-Gbaguidi. 2014. Macrophage phenotypes and their modulation in atherosclerosis. *Circ. J.* 78: 1775–1781.
21. Zhu, W., Z. Jin, J. Yu, J. Liang, Q. Yang, F. Li, X. Shi, X. Zhu, and X. Zhang. 2016. Baicalin ameliorates experimental inflammatory bowel disease through polarization of macrophages to an M2 phenotype. *Int. Immunopharmacol.* 35: 119–126.
22. Aroor, A. R., S. McKarns, V. G. Demarco, G. Jia, and J. R. Sowers. 2013. Maladaptive immune and inflammatory pathways lead to cardiovascular insulin resistance. *Metabolism* 62: 1543–1552.
23. Chalmers, S. A., V. Chitu, M. Ramanujam, and C. Putterman. 2015. Therapeutic targeting of macrophages in lupus nephritis. *Discov. Med.* 20: 43–49.
24. Huston, J. M., and K. J. Tracey. 2011. The pulse of inflammation: heart rate variability, the cholinergic anti-inflammatory pathway and implications for therapy. *J. Intern. Med.* 269: 45–53.
25. Ohashi, W., K. Hattori, and Y. Hattori. 2015. Control of macrophage dynamics as a potential therapeutic approach for clinical disorders involving chronic inflammation. *J. Pharmacol. Exp. Ther.* 354: 240–250.
26. Belliere, J., A. Casemayou, L. Ducasse, A. Zakaroff-Girard, F. Martins, J. S. Iacovoni, C. Guilbeau-Frugier, B. Buffin-Meyer, B. Pipy, D. Chauveau, et al. 2015. Specific macrophage subtypes influence the progression of rhabdomyolysis-induced kidney injury. *J. Am. Soc. Nephrol.* 26: 1363–1377.
27. Lu, L., J. Barbi, and F. Pan. 2017. The regulation of immune tolerance by FOXP3. *Nat. Rev. Immunol.* 17: 703–717.
28. Martín-Orozco, E., M. Norte-Muñoz, and J. Martínez-García. 2017. Regulatory T cells in allergy and asthma. *Front Pediatr.* 5: 117.
29. Saresella, M., I. Marventano, R. Longhi, F. Lissoni, D. Trabattoni, L. Mendozzi, D. Caputo, and M. Clerici. 2008. CD4+CD25+FoxP3+PD1- regulatory T cells in acute and stable relapsing-remitting multiple sclerosis and their modulation by therapy. *FASEB J.* 22: 3500–3508.
30. Kawai, K., M. Uchiyama, J. Hester, K. Wood, and F. Issa. 2017. Regulatory T cells for tolerance. *Hum. Immunol.* DOI: 10.1016/j.humimm.2017.12.013.
31. Qiao, Y. C., J. Shen, L. He, X. Z. Hong, F. Tian, Y. H. Pan, L. Liang, X. X. Zhang, and H. L. Zhao. 2016. Changes of regulatory T cells and of proinflammatory and immunosuppressive cytokines in patients with type 2 diabetes mellitus: a systematic review and meta-analysis. *J. Diabetes Res.* 2016: 3694957.
32. Tipton, A. J., B. Baban, and J. C. Sullivan. 2012. Female spontaneously hypertensive rats have greater renal anti-inflammatory T lymphocyte infiltration than males. *Am. J. Physiol. Regul. Integr. Comp. Physiol.* 303: R359–R367.
33. Zimmerman, M. A., B. Baban, A. J. Tipton, P. M. O'Connor, and J. C. Sullivan. 2015. Chronic ANG II infusion induces sex-specific increases in renal T cells in Sprague-Dawley rats. *Am. J. Physiol. Renal Physiol.* 308: F706–F712.
34. Gigliotti, J. C., L. Huang, H. Ye, A. Bajwa, K. Chattrabhuti, S. Lee, A. L. Klibanov, K. Kalantari, D. L. Rosin, and M. D. Okusa. 2013. Ultrasound prevents renal ischemia-reperfusion injury by stimulating the splenic cholinergic anti-inflammatory pathway. *J. Am. Soc. Nephrol.* 24: 1451–1460.
35. Dobre, M., M. Rahman, and T. H. Hostetter. 2015. Current status of bicarbonate in CKD. *J. Am. Soc. Nephrol.* 26: 515–523.
36. Lazarus, B., Y. Chen, F. P. Wilson, Y. Sang, A. R. Chang, J. Coresh, and M. E. Grams. 2016. Proton pump inhibitor use and the risk of chronic kidney disease. *JAMA Intern. Med.* 176: 238–246.
37. Martelli, D., M. J. McKinley, and R. M. McAllen. 2014. The cholinergic anti-inflammatory pathway: a critical review. *Auton. Neurosci.* 182: 65–69.
38. Kooijman, S., I. Meurs, L. van Beek, P. P. Khedoe, A. Giezekamp, K. Pike-Overzet, C. Cailotto, J. van der Vliet, V. van Harmelen, G. Boeckxstaens, et al. 2015. Splenic autonomic denervation increases inflammatory status but does not aggravate atherosclerotic lesion development. *Am. J. Physiol. Heart Circ. Physiol.* 309: H646–H654.
39. Kooijman, S., W. J. de Jonge, and P. C. Rensen. 2015. Reply to "letter to the editor: parasympathetic innervation of the rodent spleen?". *Am J Physiol Heart Circ Physiol* 309: H2159.
40. Bratton, B. O., D. Martelli, M. J. McKinley, D. Trevaks, C. R. Anderson, and R. M. McAllen. 2012. Neural regulation of inflammation: no neural connection from the vagus to splenic sympathetic neurons. *Exp. Physiol.* 97: 1180–1185.
41. Rosas-Ballina, M., P. S. Olofsson, M. Ochani, S. I. Valdés-Ferrer, Y. A. Levine, C. Reardon, M. W. Tusche, V. A. Pavlov, U. Andersson, S. Chavan, et al. 2011. Acetylcholine-synthesizing T cells relay neural signals in a vagus nerve circuit. *Science* 334: 98–101.
42. Zila, I., D. Mokra, J. Kopincova, M. Kolomaznik, M. Javorka, and A. Calkovska. 2017. Vagal-immune interactions involved in cholinergic anti-inflammatory pathway. *Physiol. Res.* 66(Suppl. 2): S139–S145.
43. Wessler, I., and C. J. Kirkpatrick. 2008. Acetylcholine beyond neurons: the non-neuronal cholinergic system in humans. *Br. J. Pharmacol.* 154: 1558–1571.
44. Trombino, S., A. Cesario, S. Margaritora, P. Granone, G. Motta, C. Falugi, and P. Russo. 2004. Alpha7-nicotinic acetylcholine receptors affect growth regulation of human mesothelioma cells: role of mitogen-activated protein kinase pathway. *Cancer Res.* 64: 135–145.
45. Mihara, T., W. Otsubo, K. Horiguchi, S. Mikawa, N. Kaji, S. Iino, H. Ozaki, and M. Hori. 2017. The anti-inflammatory pathway regulated via nicotinic acetylcholine receptors in rat intestinal mesothelial cells. *J. Vet. Med. Sci.* 79: 1795–1802.
46. Park, J. H., Y. G. Kim, M. Shaw, T. D. Kanneganti, Y. Fujimoto, K. Fukase, N. Inohara, and G. Núñez. 2007. Nod1/RICK and TLR signaling regulate chemokine and antimicrobial innate immune responses in mesothelial cells. *J. Immunol.* 179: 514–521.
47. Valle, M. T., M. L. Degl'Innocenti, R. Bertelli, P. Facchetti, F. Perfumo, D. Fenoglio, A. Kunkl, R. Gusmano, and F. Manca. 1995. Antigen-presenting function of human peritoneum mesothelial cells. *Clin. Exp. Immunol.* 101: 172–176.
48. Cailotto, C., L. M. Costes, J. van der Vliet, S. H. van Bree, J. J. van Heerikhuize, R. M. Buijs, and G. E. Boeckxstaens. 2012. Neuroanatomical evidence demonstrating the existence of the vagal anti-inflammatory reflex in the intestine. *Neurogastroenterol Motil* 24:191–200, e193.
49. Bernik, T. R., S. G. Friedman, M. Ochani, R. DiRaimo, S. Susarla, C. J. Czura, and K. J. Tracey. 2002. Cholinergic antiinflammatory pathway inhibition of tumor necrosis factor during ischemia reperfusion. *J. Vasc. Surg.* 36: 1231–1236.
50. Bernik, T. R., S. G. Friedman, M. Ochani, R. DiRaimo, L. Ulloa, H. Yang, S. Sudan, C. J. Czura, S. M. Ivanova, and K. J. Tracey. 2002. Pharmacological stimulation of the cholinergic antiinflammatory pathway. *J. Exp. Med.* 195: 781–788.
51. Kwan, H., L. Garzoni, H. L. Liu, M. Cao, A. Desrochers, G. Fecteau, P. Burns, and M. G. Frasch. 2016. Vagus nerve stimulation for treatment of inflammation: systematic review of animal models and clinical studies. *Bioelectron. Med.* 3: 1–6.
52. Matteoli, G., and G. E. Boeckxstaens. 2013. The vagal innervation of the gut and immune homeostasis. *Gut* 62: 1214–1222.
53. Berthoud, H. R., W. B. Laughton, and T. L. Powley. 1986. Vagal stimulation-induced gastric acid secretion in the anesthetized rat. *J. Auton. Nerv. Syst.* 16: 193–204.
54. Okuma, Y., and Y. Osumi. 1986. Central cholinergic descending pathway to the dorsal motor nucleus of the vagus in regulation of gastric functions. *Jpn. J. Pharmacol.* 41: 373–379.
55. Pevsner, L., and M. I. Grossman. 1955. The mechanism of vagal stimulation of gastric acid secretion. *Gastroenterology* 28:493–499; discussion, 531–495.
56. Mao, Y., T. Tokudome, I. Kishimoto, K. Otani, H. Nishimura, O. Yamaguchi, K. Otsu, M. Miyazato, and K. Kangawa. 2015. Endogenous ghrelin attenuates pressure overload-induced cardiac hypertrophy via a cholinergic anti-inflammatory pathway. *Hypertension* 65: 1238–1244.
57. Bellinger, D. L., D. Lorton, R. W. Hamill, S. Y. Felten, and D. L. Felten. 1993. Acetylcholinesterase staining and choline acetyltransferase activity in the young adult rat spleen: lack of evidence for cholinergic innervation. *Brain Behav. Immun.* 7: 191–204.
58. Elfvin, L. G., J. Johansson, A. S. Höijer, and H. Aldskogius. 1994. The innervation of the splenic capsule in the guinea pig: an immunohistochemical and ultrastructural study. *J. Anat.* 185: 267–278.
59. Tipton, A. J., B. Baban, and J. C. Sullivan. 2014. Female spontaneously hypertensive rats have a compensatory increase in renal regulatory T cells in response to elevations in blood pressure. *Hypertension* 64: 557–564.
60. Dick, A. D., A. L. Ford, J. V. Forrester, and J. D. Sedgwick. 1995. Flow cytometric identification of a minority population of MHC class II positive cells in the normal rat retina distinct from CD45lowCD11b/c+CD4low parenchymal microglia. *Br. J. Ophthalmol.* 79: 834–840.
61. He, J., Y. Yin, T. A. Luster, L. Watkins, and P. E. Thorpe. 2009. Anti-phosphatidylserine antibody combined with irradiation damages tumor blood vessels and induces tumor immunity in a rat model of glioblastoma. *Clin. Cancer Res.* 15: 6871–6880.
62. Kato, M., S. Khan, E. d'Aniello, K. J. McDonald, and D. N. Hart. 2007. The novel endocytic and phagocytic C-type lectin receptor DCL-1/CD302 on macrophages is colocalized with F-actin, suggesting a role in cell adhesion and migration. *J. Immunol.* 179: 6052–6063.
63. Yokoyama, W. M., F. Koning, P. J. Kehn, G. M. Pereira, G. Stingl, J. E. Coligan, and E. M. Shevach. 1988. Characterization of a cell surface-expressed disulfide-linked dimer involved in murine T cell activation. *J. Immunol.* 141: 369–376.
64. Baban, B., J. Y. Liu, X. Qin, N. L. Weintraub, and M. S. Mozaffari. 2015. Upregulation of programmed death-1 and its ligand in cardiac injury models: interaction with GADD153. *PLoS One* 10: e0124059.
65. Glorie, L. L., A. Verhulst, V. Matheeussen, L. Baerts, J. Magielse, N. Hermans, P. C. D'Haese, I. De Meester, and A. De Beuf. 2012. DPP4 inhibition improves functional outcome after renal ischemia-reperfusion injury. *Am. J. Physiol. Renal Physiol.* 303: F681–F688.
66. Park, E. S., K. Uchida, and H. Nakayama. 2014. Establishment of a rat model for canine necrotizing meningoencephalitis (NME). *Vet. Pathol.* 51: 1151–1164.
67. Baban, B., A. M. Hansen, P. R. Chandler, A. Manlapat, A. Bingaman, D. J. Kahler, D. H. Munn, and A. L. Mellor. 2005. A minor population of splenic

dendritic cells expressing CD19 mediates IDO-dependent T cell suppression via type I IFN signaling following B7 ligation. *Int. Immunol.* 17: 909–919.
68. Kishimoto, T. ed. 1996. Leucocyte typing VI: white cell differentiation antigens. In *6th International Workshop and Conference on Human Leucocyte Differentiation Antigens.* Garland Publishing, Kobe, Japan.
69. Chirkova, T., S. Boyoglu-Barnum, K. A. Gaston, F. M. Malik, S. P. Trau, A. G. Oomens, and L. J. Anderson. 2013. Respiratory syncytial virus G protein CX3C motif impairs human airway epithelial and immune cell responses. *J. Virol.* 87: 13466–13479.
70. Le Cabec, V., L. J. Emorine, I. Toesca, C. Cougoule, and I. Maridonneau-Parini. 2005. The human macrophage mannose receptor is not a professional phagocytic receptor. *J. Leukoc. Biol.* 77: 934–943.
71. Abrams, J. S., M. G. Roncarolo, H. Yssel, U. Andersson, G. J. Gleich, and J. E. Silver. 1992. Strategies of anti-cytokine monoclonal antibody development: immunoassay of IL-10 and IL-5 in clinical samples. *Immunol. Rev.* 127: 5–24.
72. Chen, G., S. Nie, C. Han, K. Ma, Y. Xu, Z. Zhang, S. M. Papa, and X. Cao. 2017. Antidyskinetic effects of MEK inhibitor are associated with multiple neurochemical alterations in the striatum of hemiparkinsonian rats. *Front. Neurosci.* 11: 112.